

PEXMOD Technical Report: Starting Point report of Component C1, C2 & C3

Summarizing and integrating existing knowledge from
completed analyses of ENRECA-3 samples –
the starting point and working hypotheses

Compiled by Lars Henrik Nielsen, Jussi Hovikoski
and the ENRECA team



PEXMOD Technical Report: Starting Point report of Component C1, C2 & C3

Summarizing and integrating existing knowledge from
completed analyses of ENRECA-3 samples –
the starting point and working hypotheses

Compiled by Lars Henrik Nielsen, Jussi Hovikoski
and the ENRECA team

1.	Resume	3
2.	Introduction	5
2.1.	Geological setting	5
2.2.	Exploration summary	8
3.	Material and Methods	13
3.1.	Core well and its location	13
3.2.	Sampling Strategy and Investigations	13
4.	Resume of conducted analyses	16
4.1.	Biostratigraphic and palynofacies analyses.....	16
4.2.	HH-XRF and Isotope analyses.....	16
4.3.	Sedimentary facies	18
4.4.	Source Rock Screening and Biomarker analyses.....	20
4.6.	Petrography.....	21
5.	Discussion – implications, hypotheses and future studies	23
5.1.	Depositional evolution and sedimentary facies.....	23
5.2.	Sandstone Petrography	24
5.3.	Poro-perm analyses.....	24
5.4.	Structural-Depositional model	24
5.5.	Implications for exploration	25
6.	Conclusions	26
7.	Acknowledgement	27
8.	References	28
9.	Appendix A: Core Photos	31
10.	Appendix B: Hovikoski et al. (2016)	32

1. Resume

The Vietnamese Bach Long Vi Graben is located in the Gulf of Tonkin near the intersection between the Song Hong and Beibuwan basins and linking the two basins. Owing to very pronounced inversion tectonic movements, part of the deeply buried rift succession is exposed on the remote Bach Long Vi Island that delineates the crest of the intra-basinal Neogene inversion structure. The island and the sea-bottom around it expose oil-prone mudstones and offer a unique geological window into the otherwise deeply buried Paleogene syn-rift succession containing matured source rock facies in places in the two basins. In order to study in detail the depositional evolution of the syn-rift succession formed during the rift climax the ENRECA project decided to drill a stratigraphic research core well, ENRECA-3, on the island in 2013. The well obtained 500 m of high-quality continuous cores consisting of lacustrine mudstones interbedded with various types of density flow facies that range from mm- and cm-scale, mud-rich density flow deposits to m-scale classic hybrid beds showing the typical bed motifs known from marine hybrid event beds. The mudstones form excellent to good oil source rocks with a cumulative thickness of minimum 233 m with an average TOC content of 2.91 wt.% and an average HI of 575 mg HC/g TOC. The interbedded sandstones constituting potential migration paths and reservoirs are quartz-rich, very fine to coarse-grained sandstone with dominantly angular–subrounded grains, mostly moderate to well-sorted arkoses with 10–22% gas porosity and Klinkenberg permeabilities of 0.1–38 mDarcy excluding the tight debrites. Bioturbation is almost absent except for tiny shallow burrows related to the gravity flows. Only freshwater palynomorphs are found and the Sulphur content is low. Soft sediment de-formation structures including ball and pillow structures, mud-flames, sand injectites and deformed rip-up mud clasts are very common. Detailed biomarker analyses of mudstone laminae and mudstone clasts in density flow beds reveal generally no significant terrestrial organic input.

The analyses thus indicate that deposition occurred in a deep, elongated, narrow subsiding freshwater graben system where mud accumulated on a soft, oxygen-poor lake bottom. Mud-rich flows and sand-dominated density flows possibly originated from graben margin aprons that owing to tectonically-induced slope instability delivered sediment flows that rapidly decelerated due to gradient change, high sediment concentration and the fluid mud prone lake floor. In combination with evidence from the studied seismic and well data it is suggested that source rock pods were mainly generated and preserved in areas with prolific algae production, limited fluvial sediment input and increased subsidence. In such

settings, even very thick, highly oil-prone lacustrine successions may form as shown by the cored succession.

2. Introduction

2.1. Geological setting

Many oil fields, particularly in Asia are charged from lacustrine and coaly source rocks contained within the syn-rift succession (e.g. Williams et al., 1995; Todd et al., 1997). Despite their importance for hydrocarbon plays, relatively few studies document in detail the depositional processes and the relationship between the mudstones and their inter-bedded facies. This is owing to the typical occurrence in deep offshore basins, such as the Paleogene basins in Asia and the scarcity of well-exposed sections. Much of the previous work on these systems is therefore based on relatively poor resolution well and seismic data and modern analogues. Although the general factors (e.g. climate, subsidence, reduced clastic input, water stratification, anoxia) controlling the development of the source rocks are well understood, the distribution of prolific source rock pods within rift systems is inadequately understood imposing exploration risks. This was realized during the early exploration phases and several geological models describing generation of non-marine source rocks have been proposed (e.g. Lambiase 1990; Lambiase & Bosworth 1995; Prosser 1993; Nottvedt et al., 1995; Katz 1995; Sladen 1997; Bohacs et al. 2000; Gawthorpe and Leeder 2000). Exploration efforts in the Cenozoic basins located on the Vietnamese shelf area have documented thick sedimentary successions overlying pre-Cenozoic strata and crystalline basement (Fig. 1). Here the Paleogene syn-rift successions mainly consist of alluvial and fluvial coarse-grained clastics, lacustrine mudstones and coaly beds and marginal marine sediments. The exploration results have demonstrated that the hydrocarbon plays rely on syn-rift lacustrine mudstones and coaly beds as the principal source rocks. However, unsuccessful wells are still commonly drilled and successful exploration seems hampered by an insufficient understanding of the governing factors for generation and distribution of the prolific source rock pods. This may in part owe to relatively low resolution exploration data such as seismic data and fairly scattered well data primarily from structural highs and with limited cores, as well as the shortage of well-exposed syn-rift successions, which hinders detailed investigations of the nature of the source rock bearing successions. The drilling of unsuccessful exploration wells illustrates the inadequate ability of current exploration models to predict distribution of mature source rock pods, migration paths and presence of reservoirs with sufficient accuracy.

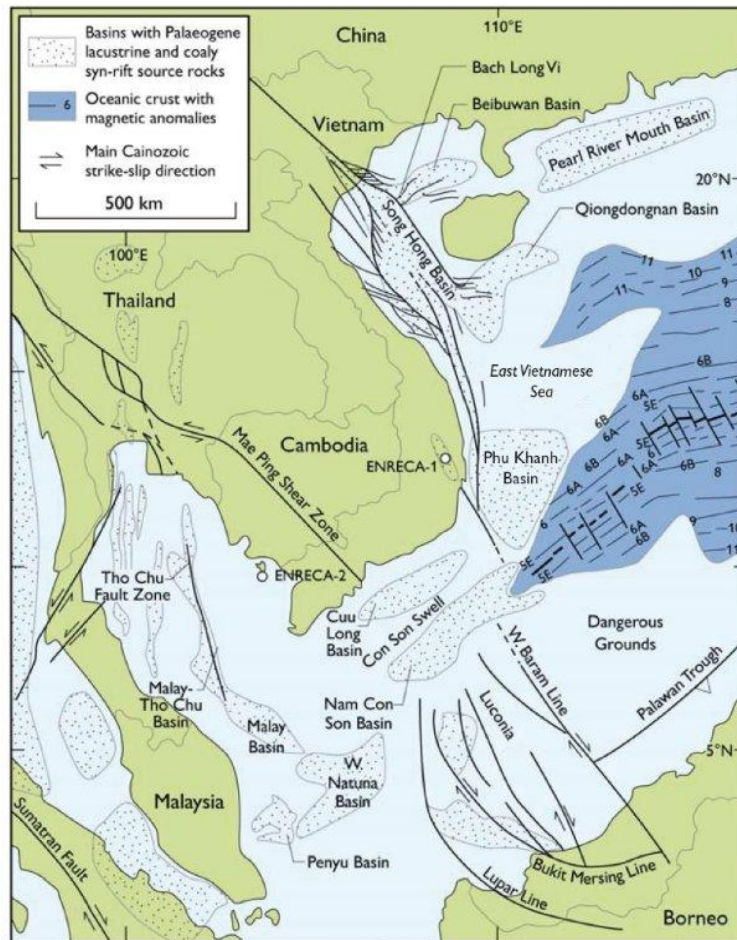


Figure 1. Map showing the principal Cenozoic structures and offshore rift basins along the Vietnamese margin and neighbouring areas. The positions of the ENRECA-1, -2 and -3 core wells are indicated.

Comprehensive reviews of rift lake basins and their petroleum systems recognise a number of characteristic development trends and classification schemes such as a typical tri-partite structural basin development with an early, maximum and late rift evolution. The structural relation between sediment input and formation of accommodation space causes basins to be under filled, balanced or overfilled, and a general discrimination of three major types of lacustrine facies associations (fluvial-lacustrine, fluctuating profundal, evaporitic) (e.g. Lambiase 1990; Prosser 1993; Nottvedt et al., 1995; Katz 1995; Sladen 1997; Bohacs et al. 2000; Gawthorpe and Leeder 2000). Based on their study of commercial occurrences of lacustrine systems Bohacs et al. (2000) addressed some key exploration challenges such as distribution of source, seal and reservoir rocks, and presented a framework for the development of predictive models. This report, summarizing the preliminary findings of the ENRECA-3 project, is aiming to present the starting point for the new PEXMOD project.

The PEXMOD project is aiming toward an integrated exploration model based on the integration of a number of geological-geophysical disciplines including seismic structural mapping, seismic facies analyses, detailed sedimentological core logging and facies analyses, well-log analysis, source rock and biomarker analyses, sandstone petrography and diageneses, porosity-permeability measurements, clay mineralogy and biostratigraphic analyses.

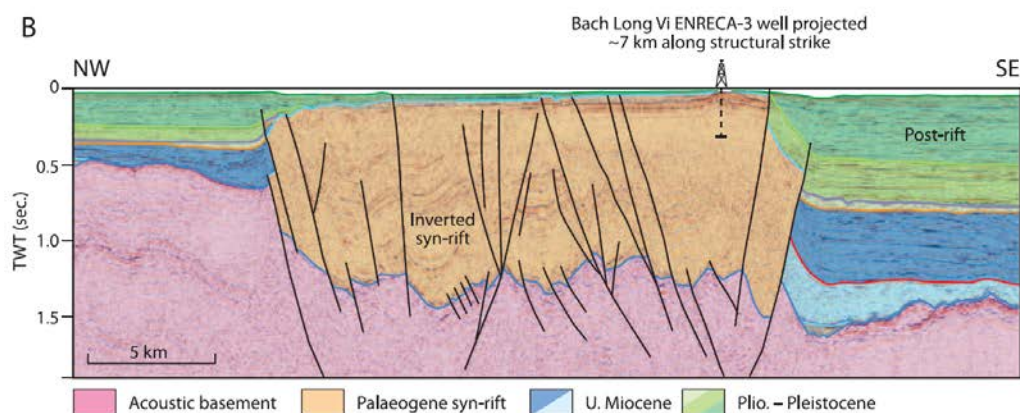
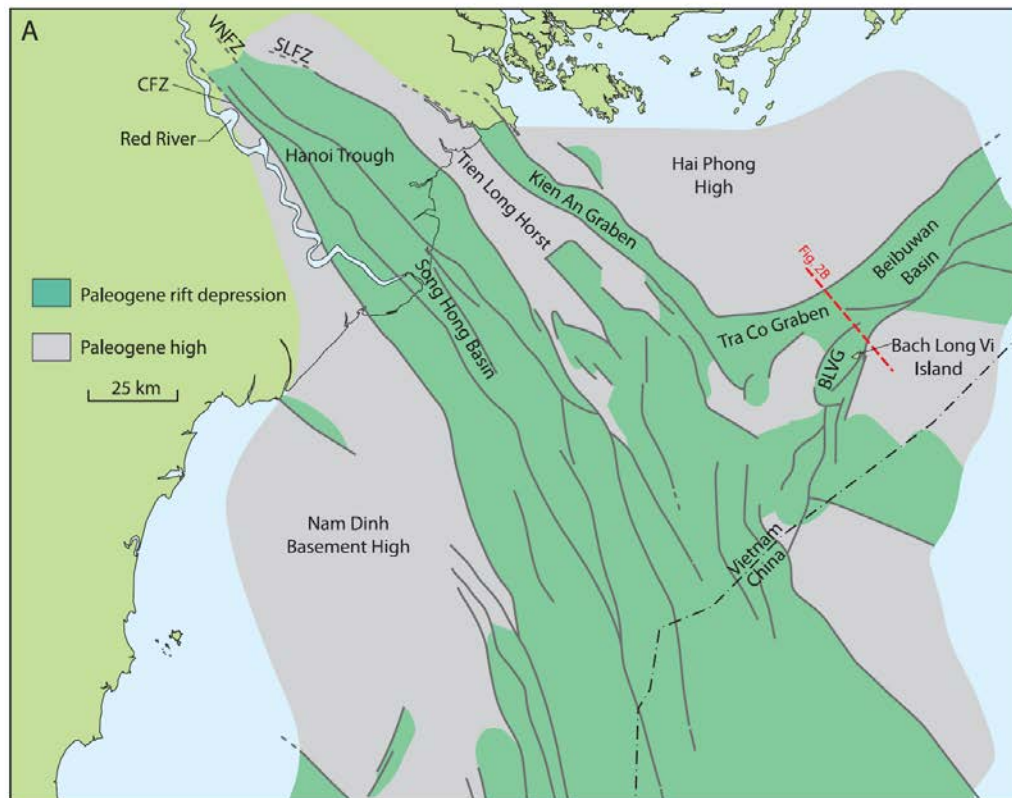


Figure 2 (Previous page). A) Map showing the outline of the Song Hong Basin, offshore northern Vietnam. The location of the Bach Long Vi Island, the main Paleogene faults, rift depressions, and structural highs are emphasized. Bold red line indicates the position of Part B. BLVG, Bach long Vi Graben; CFZ, Chay Fault Zone; SLFZ, Song Lo Fault Zone; VNFZ, Vinh Ninh Fault Zone. B) A NW–SE seismic section and interpreted geo-section displaying the significantly inverted Bach Long Vi Graben. The relative position of the ENRECA-3 core well is projected into the geo-section.

2.2. Exploration summary

Petroleum exploration in the North Song Hong Basin started in the late 1970s with analogue seismic acquisition and 2D regional seismic surveys. The first exploration well drilled in the area was by Total in the 1990s. Since then, a large amount of seismic and well data has been collected over the years through various exploration activities by different operators (Figs 3 and 4). Based on these results, it is clear that structural and tectonic elements strongly influence the kind of play and expected petroleum system in the area (Fig. 5). Therefore, this report attempts to categorize the exploration results according to structural elements of the study area, which consists of three sectors: The Central Sector (a.k.a. Miocene Inversion Zone), the Eastern Sector (a.k.a. NE Song Lo Fault Differentiated Zone), and the West Beibuwan Sector.

2.2.1. Central Sector

Exploration in this area primarily targets the Miocene inverted structures with Miocene-Oligocene clastic reservoirs. Many wells have been drilled in the area, and all of the discoveries made have been gas. During 1990-2000, 4 wells were drilled in the area with either sub-commercial discovery, gas show or dry (103T-H-1X, 103T-G-1X, 102-HD-1X, 102-CQ-1X, 103-HOL-1X).

The first encouraging exploration results was in 2006 with 103-BAL-1X. The well encountered two gas sands in the Middle Miocene with 8.46 mmscfpd and 16.8 mmscfpd of gas flow. Since then, a series of gas discoveries were made over the years: 102-TB-1X in 2006, 103-DL-1X in 2009, and most recently 107-KL-1X in 2015. The only failed well was 102/10-SP-1X in 2014. Most of the discovery wells have gas flow in the Miocene sands ranging from 16.2 to 24 mmscfpd. The most recent well 107-KL-1X also yield condensate flow of 194.3 bpd in addition to gas flow of 6.24 to 7.7 mmscfpd. Oligocene clastic targets remain

unproven, as most of the wells do not penetrate the interval, or the results are either dry, gas shows or tight gas reservoir.

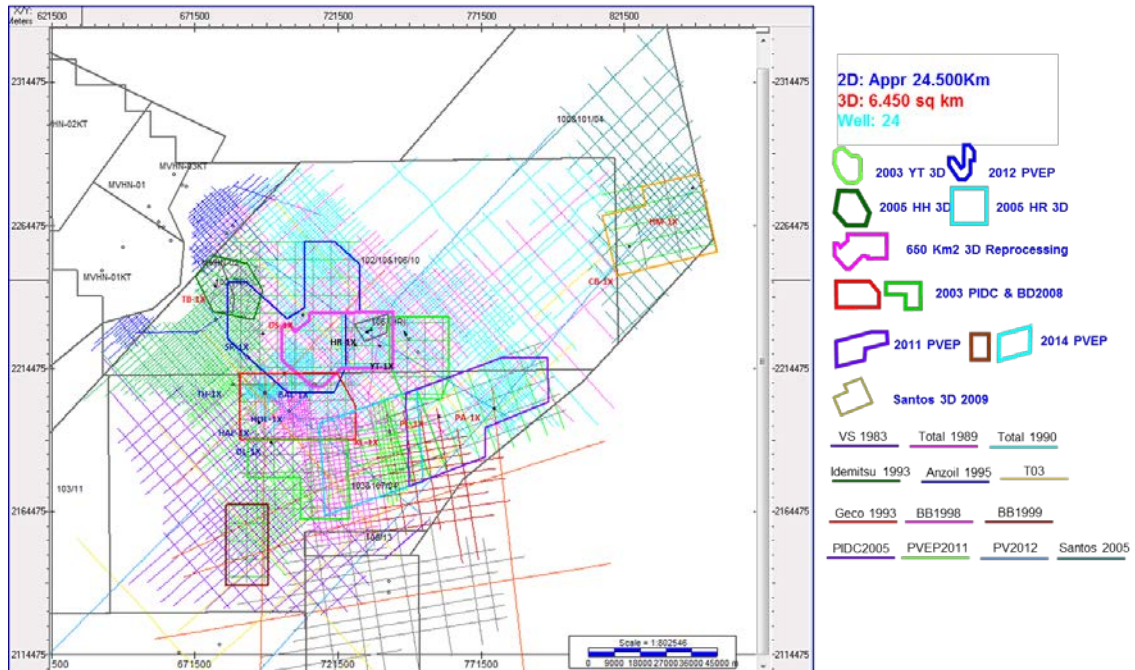


Figure 3. Seismic acquisition activities in the study area.

2.2.2. Eastern Sector

The main exploration targets in this area are the Pre-Tertiary fractured carbonate basement and Miocene-Oligocene clastic reservoirs. Discoveries are generally oil and gas in fractured carbonate basement, and mostly concentrated to the West of the Bach Long Vy basement high. Some gas discoveries are made in the Miocene and Oligocene targets, but generally they are secondary to the basement play.

106-Yen Tu-1X (September 2004) is the first well drilled in the area, targeting the pre-Tertiary fractured/karstified carbonate rock play and Miocene/Oligocene stratigraphic plays. It encountered 2.9m of net oil in Middle Miocene sand with average porosity of 18.0% and average Sw of 57.0%. The well became the first oil discovery in offshore Northern Vietnam and also has proven the presence of oil in the Song Hong basin.

Following this positive discovery, 8 exploration wells are drilled in the period 2006-2015 which primarily target the fractured carbonate basement, with the Oligocene-Miocene clas-

tics as secondary targets. Most of these discoveries are in the fracture basement only: 106-HR-1X (Ham Rong structure, 2008) with 4859 bpd oil flow and 7 mmscfd gas flow; 106-HR-2X (2009) with 3401 bpd oil flow and 4.47 mmscfd gas flow; and 106-HRN (Ham Rong Nam structure, 2013) with 2390 bpd condensate flow and 22.9 mmscfd gas flow.

In 2014, the well 106/10-HRD-1X (Ham Rong Dong) encountered oil and gas both in the fractured carbonate basement and in the Oligocene section. Two DSTs were carried out: DST#1 in carbonate basement yielded gas flowrate at 13.7 mmsc/d & condensate 895 bpd; DST#2 in Oligocene interval yielded gas flow at 30.5 mmscfd & condensate 2391 bpd.

Exploration in the area is certainly not without negative results:

- 106-HL-1X was drilled in 2006 targeting the fractured carbonate basement and Miocene-Oligocene clastic play, and only encountered oil shows. However several oil and gas discoveries are made subsequently nearby (HR, HRD and HRN).
- 106-YT-2X was drilled in 2009, following the 106-YT-1X discovery in 2004, to appraise the Yen Tu structure and it was plugged and abandoned without HC show in Carbonate reservoir and high water saturation in Miocene sandstone.
- 106-DS-1X is an attempt away from the Ham Rong-Yen Tu area, and still target primarily the fractured carbonate basement. However, the well was dry after disappointing testing result.
- 106/10-HRD-2X well was drilled in 2015 following the success of the 106/10-HRD-1X to appraise the potential of the Oligocene clastic reservoir. However, the well encountered Oligocene sands with weak HC shows, and no DST tests are conducted.

2.2.3. West Beibuwan Sector

Exploration activities in the area started in the 1990 with the drilling of well 197T-PA-1X by Total. Since then there have been a total of 6 exploration wells in the area. These wells mainly target three different plays: fractured carbonate basement, Oligocene clastic, and Miocene clastic reservoirs.

In contrast to the Eastern Sector, fractured carbonate basement play is unproven so far in the area. Despite earlier success to the West of the Bach Long Vy Basement high

(BLVBH), 107-PL-1X was drilled immediately to the South of the structural high and encountered only oil and gas show in the basement. 101-CB-1X targeted carbonate basement to the NE of the BLVBM, but only encountered dry clastic basement.

Oligocene clastic reservoirs in inverted rift structures are popular targets in the area. 197T-PA-1X targeted an Oligocene inversion structure to the South of the BLVBH, but the well was dry. WZ 14-2-1 (1991) was a discovery well by CNOOC in the Oligocene sandstone, trapped in a late Miocene-Pliocene inversion structure in the Bach Long Vy Graben system. The test results show 12-15 mmscfd gas flow and 57 bpd condensate flow. However WZ 14-2-2 appraisal well for the same structure was a dry hole without any tests. 101-HM-1X (2009) was another well nearby targeting a similar kind of structure and encountered 5 gas pay intervals in Oligocene sandstone without any DSTs.

Miocene targets are generally secondary in the area. The only well with HC is 107-PL-1X, which encountered oil and gas in the Upper Miocene.

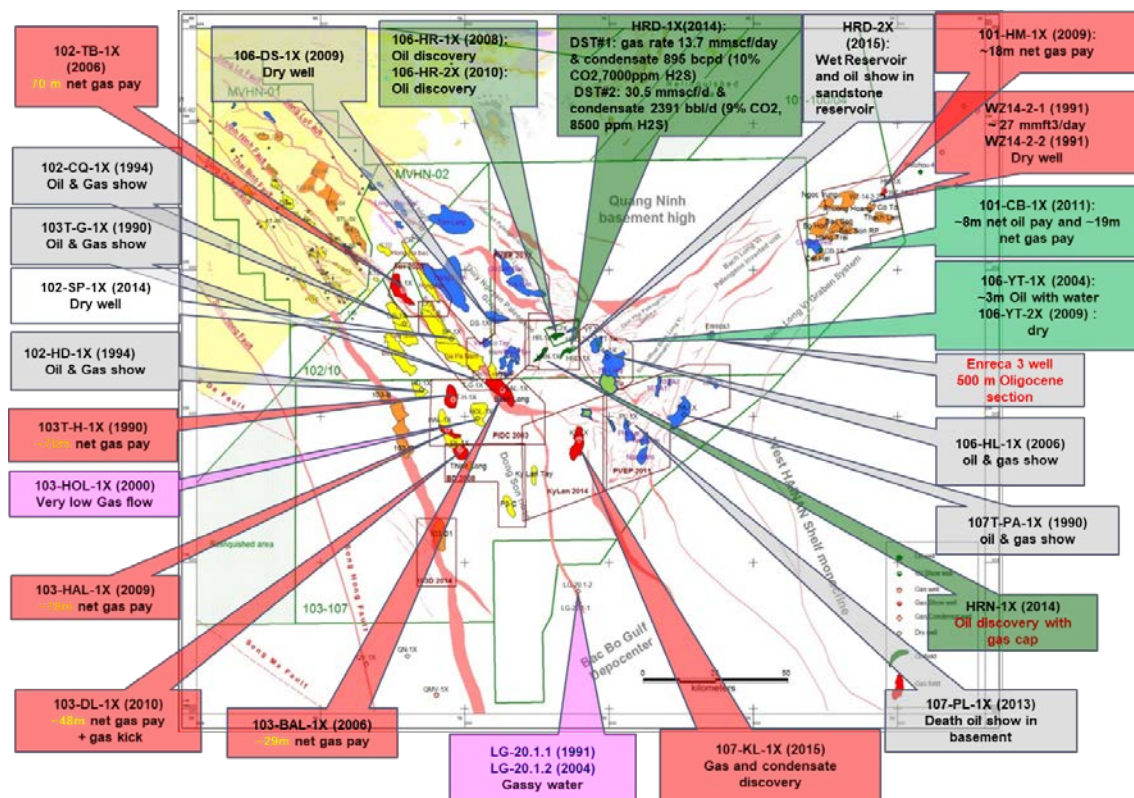


Figure 4. Exploration well results in the study area.

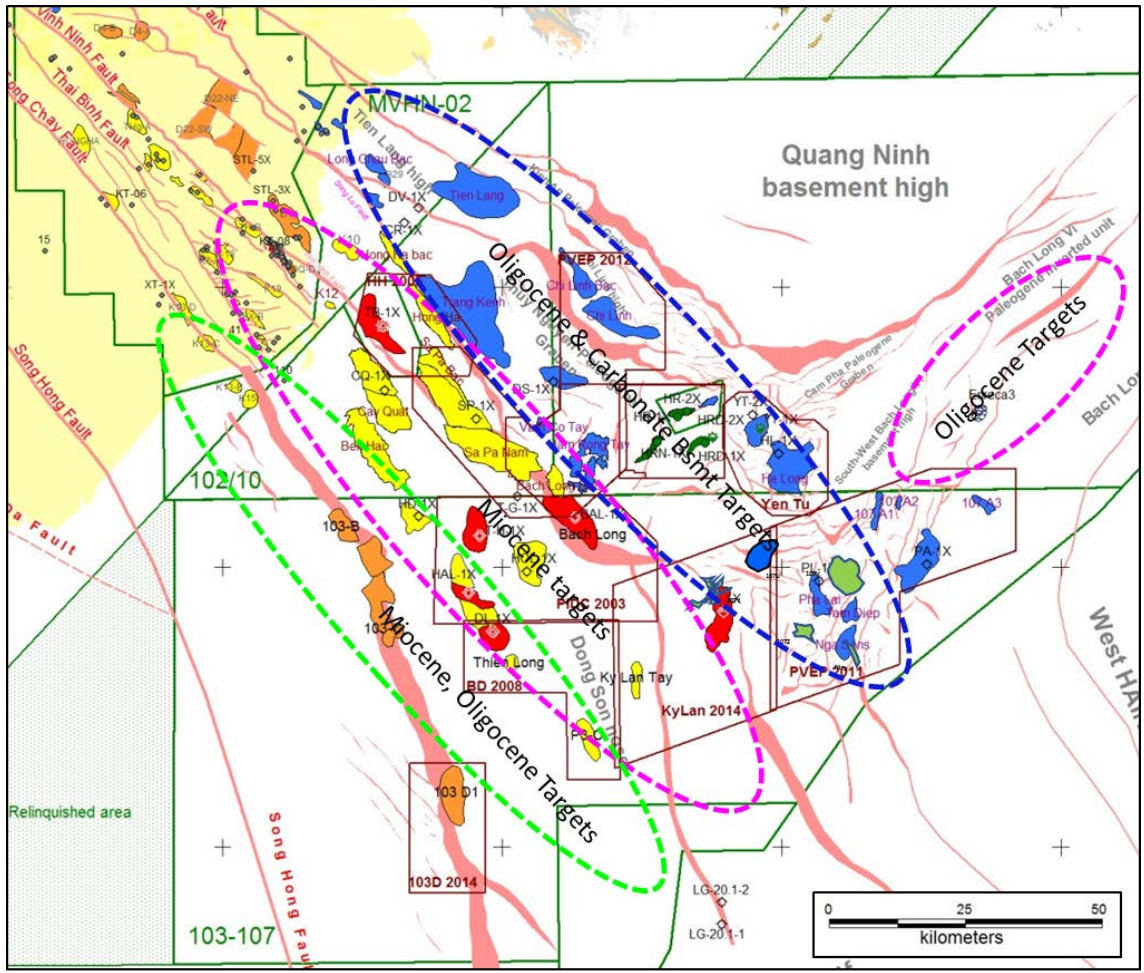


Figure 5. Exploration targets in the study area

3. Material and Methods

3.1. Core well and its location

The small island of Bach Long Vi constituting the topmost part of a large Neogene inversion structure near the intersection of the Song Hong and Beibuwan basins exposes syn-rift sedimentary strata. The island thus offers a unique geological window into the otherwise deeply buried Paleogene syn-rift succession of the two basins. The strata is exposed in the tidal zone and shows gently dipping alternating sandstones and light grey mudstones that in several places are intruded and cut by sandstone injectites forming irregular deformed layers and straight dykes. Initial sampling by VPI of the exposed strata on the island and the shallow sea-bottom around the island supplemented by further samples clearly indicate that the heterogeneous succession of sandstones and mudstones has an oil generative potential (Fig. 6). The mapped structural dip of the exposed strata shows a general NW gentle dip of a few degrees and up to 20 degrees. Joints and faults in addition to very gentle folds and the sandstone injectites disturbs bedding locally, but based on the general dip the ENRECA-3 well was placed in the SE-most part of the island to minimize overlap with the exposed strata.

The drilling campaign was performed in spring 2012. Gamma-ray and resistivity wire line logs were subsequently acquired. The core recovery is ca. 99% with only small parts being broken into rubble at the time of inspection. The excellent core was stored in metal boxes numbered with depths and containing 5 times 1 m of core. Selected core pieces are numbered and marked with arrows pointing down hole. The initial core facies logging defining sample strategy was performed on full un-slapped cores with minor portions slapped for detailed inspection. A large number of selected core pieces, 10-60 cm long were slapped and brought to GEUS labs for further investigations. All core boxes were photographed (Nielsen 2013; Appendix A).

3.2. Sampling Strategy and Investigations

The initial stratigraphic-sedimentological core logging in scale 1:100 revealed a continuous succession of uniformly gentle, 4–7° dipping strata dominated by deep freshwater, lacustrine basinal mudstones and siltstones interbedded with various types of density flow event

beds encompassing mud flows, low and high density turbidites, hybrid event beds and debrites. Larger dips are only observed at mudstone-sandstone contacts, and are interpreted as deformation owing to loading of sand into soft mud, sand intrusion forming common injectites, in places reinforced by differential compaction of the sand and mud. Silty-sandy event beds occur both as single beds scattered within thick mudstones units, and form packages comprising stacks of few event beds up to several m thick stacks of numerous successive events. The 500 m thick succession shows no evidence of shallow water coastal, fluvial, floodplain or swamp deposition and no macro fossils or large trace fossils have been found. Dispersed organic material is very common occasionally making sandstones and siltstones dark grey; deformed fragments of coalified terrestrial plant material, mostly less than a few centimetre are common including delicate remains of leaves. No evidence for significant faulting or displacement are found in the cores and the succession is thus interpreted to represent one continuously formed succession.

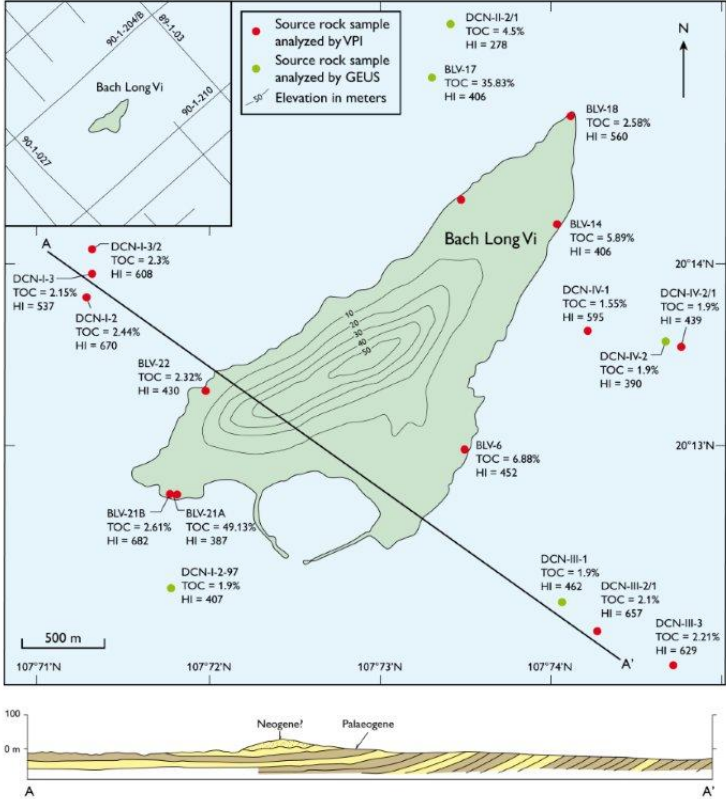


Figure 6. A) The general outline of the Bach Long Vi Island, orientation of the dipping strata and position of source rock samples. The ENRECA-3 well was placed in the SW-most part of the island to maximise the stratigraphic information further to the outcrop data. B) Simplified NW–SE cross-section across the island and adjacent offshore areas.

Based on these observations a comprehensive investigation programme was initiated with reference to the sedimentological core log. The program encompasses approximately 320 samples of mudstones for source rock screening, 26 mudstone samples for biostratigraphic analyses at VPI Labs and approximately 25 samples for the lab at GEUS, 10 samples for vitrinite reflectances, 10 mudstone samples for clay mineralogy, 24 sandstone samples for determination of porosity and permeability and 10 samples for sandstone petrography. This initial investigation programme has later been supplemented by a wide-ranging analytical program including well-log interpretation, analyses of palynofacies, maceral types, biomarker composition, analyses of siderite nodules and layers, samples for detrital zircon ages and additional source rock screening of specific mudstone layers and clasts for supporting detailed sedimentological interpretations. Furthermore, a very comprehensive geochemical analytical program encompassing carbon isotope studies of whole rock samples and terrestrial organic matter, measurement of 30+ elements by handheld XRF at approx. 2464 levels. Most of the results are still to be interpreted and integrated and will be reported in future papers.

4. Resume of conducted analyses

4.1. Biostratigraphic and palynofacies analyses

The 500 m cored succession was attempted to be dated by biostratigraphy and two sets of samples were collected. An initial set of 26 samples were analyzed for microfossils, nanofossils and palynomorphs (VPI 2013), and these were later supplemented by analysis of approximately 25 samples for palynomorphs at GEUS. The analyses did not reveal any microfossils or nanofossils. The dominating kerogen consists of degraded amorphous organic debris making the biostratigraphic dating difficult. Thus the age determination is based on relatively few *Verrutricolporites pachydermus* and *Gothanipollis basensis* pollen grains indicating the *Verrutricolporites pachydermus* sub-zone which is tentatively referred to a Late Oligocene age. In addition freshwater dinoflagellates (*Bosedinia*), fresh-water green algae such as *Botryococcus* and *Pediastrum* occur. Based on the composition of the palynomorph assemblage and the dominating amount of amorphous organic matter, a deep lacustrine depositional environment is indicated.

4.2. HH-XRF and Isotope analyses

The aim of the HH-XRF and isotope studies is to improve the understanding and interpretation of the depositional environment of the late Oligocene lacustrine organic rich oil-prone source rock succession drilled in the Enreca-3 core. On going work is made to present a combined HH-XRF-XRD data set constructed from multivariate data analysis and regression models. This data set will be used to type the rock and to predict the XRD mineral composition based on HH-XRF composition. The rock types and the modelled mineral composition highlight the geochemical variations of the sediment and allows for direct comparison with sedimentological processes and facies changes. The modeling also depicts the cyclic alteration of rock types that are present on many different scales ranging from centimeters to hundreds of meters (Fig. 7).

The sedimentological and geochemical variations observed throughout the cored section reflects fluctuating paleoclimate, tectonism and hinterland condition controlling the depositional setting, which may provide a deeper understanding of the deposition of this and simi-

lar Paleogene syn-rift succession in the region. It allows furthermore the development of a more generalized depositional model relevant for other deep-lacustrine syn-rift basins.

In addition to the HH-XRF data set, we also prepare a high-resolution stable isotope record based on bulk organic matter ($\delta^{13}\text{C}_{\text{org}}$) and fossil wood ($\delta^{13}\text{C}_{\text{wood}}$). Again in this study we make benefit of the sediments that are exceptionally well preserved. They are thus excellently suited for a detailed stratigraphical analysis of the stable isotope record and as proxy for environmental and climatic changes within this period. The density-flow deposits contain abundant fragments of fossil wood. Therefore it was possible to obtain 262 coalified wood fragments together with 1063 bulk organic samples throughout the span of the core. This allowed to establish a high resolution stable C isotope record ($\delta^{13}\text{C}_{\text{org}}$ and $\delta^{13}\text{C}_{\text{wood}}$).

The organic carbon isotope trend from the 500 m core succession provides insight into the palaeoenvironmental changes of the lake during the Oligocene. Both, global and local factors control the $\delta^{13}\text{C}$ variations. The aim of the study is to obtain pure global $\delta^{13}\text{C}_{\text{org}}$ and $\delta^{13}\text{C}_{\text{wood}}$ signals that would allow comparison of the studied sediments with coeval syn-rift successions in the South China Sea region and other parts of the world.

4.2.1. Data and Methods

In the period from August 2016 and to June 2017 analysis of the collected XRF measurements has been done. A total of 2464 hand held (HH)-XRF measurements were made systematically on the 500 m long core. To allow interpretation of the data additional XRD measurements of representative samples (16 samples) have been made at the beginning of 2017. For preparation of samples to isotope analysis, each of the samples collected in Hanoi was crushed with a hand drill or rotary crusher and later decarbonated. This allowed for determination of the amount of carbonates in the samples. Afterwards measurements of the TOC and TS have been made. All those procedures were necessary to calculate the proper amount of the sample needed to be prepared for the organic carbon isotope measurements.

The mass-spectrometry measurement (organic carbon isotope) of the samples is scheduled to be completed in February 2018. Around 1000 samples are planned for measurement.

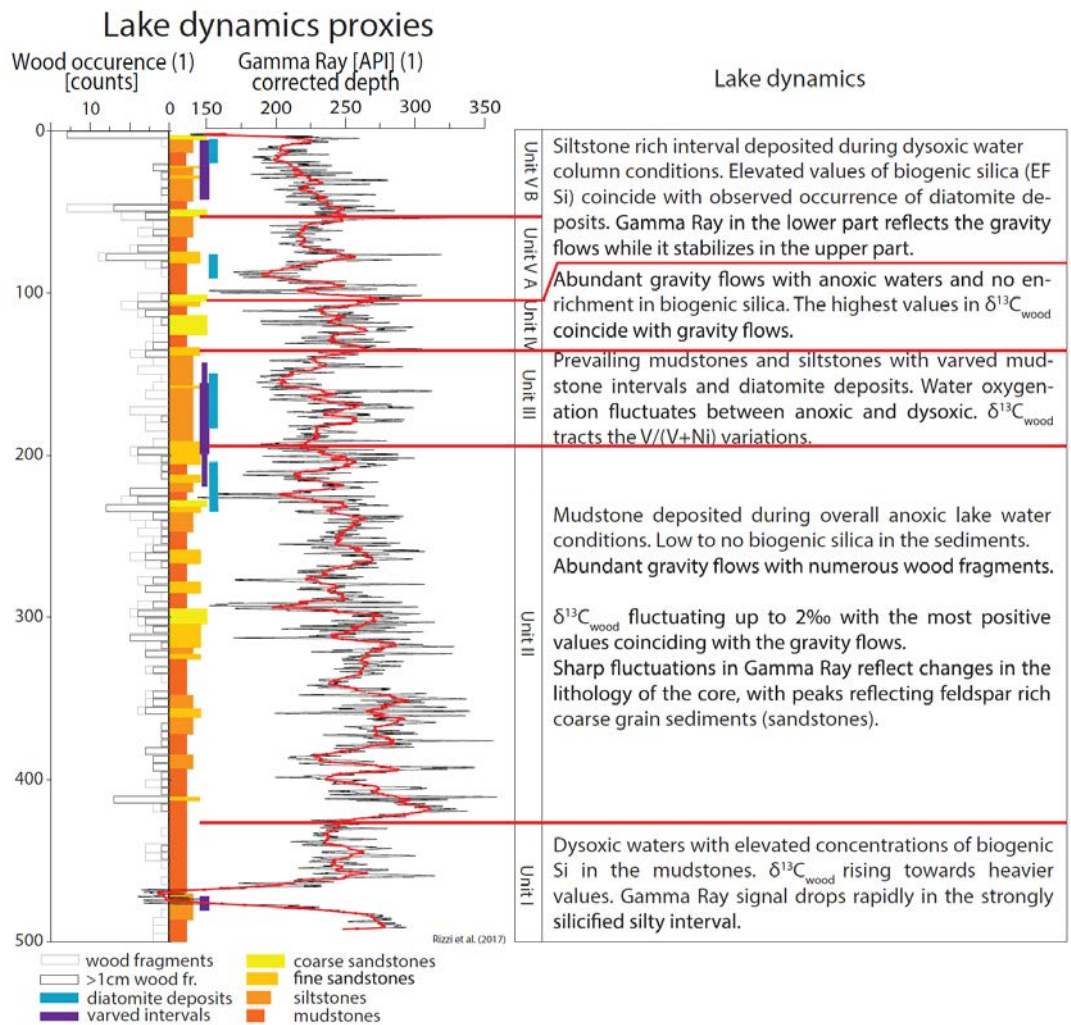


Figure 7. GR-log and log unit division derived from HH-XRF data.

4.3. Sedimentary facies

To date, sedimentological work on Enreca-3 has centred on delineating sediment transport and accumulation processes of gravity flow facies (Nielsen et al., 2014; Hovikoski et al., 2016; Appendix B). The results indicate that the Enreca-3 core records a variety of density-flow bed types that range from centimeter-scale, mud-rich density-flow deposits to meter-scale hybrid beds (*i.e.*, deposits showing change in flow type from turbidity current to debris flow during a single flow event), debrites and deposits of high-density turbidites (Fig. 8). In addition, the Enreca-3 deposits are characterized by a wide range of transitional-flow facies at various scales.

Source-rock screening data and sedimentological observations indicate that the lake floor consisted typically of water-rich mud, which was assimilated into overriding density flows. This process was probably central in modulating flow turbulence and explains the pervasive occurrence of transitional-flow facies and development of hybrid event beds via late-stage flow concentration.

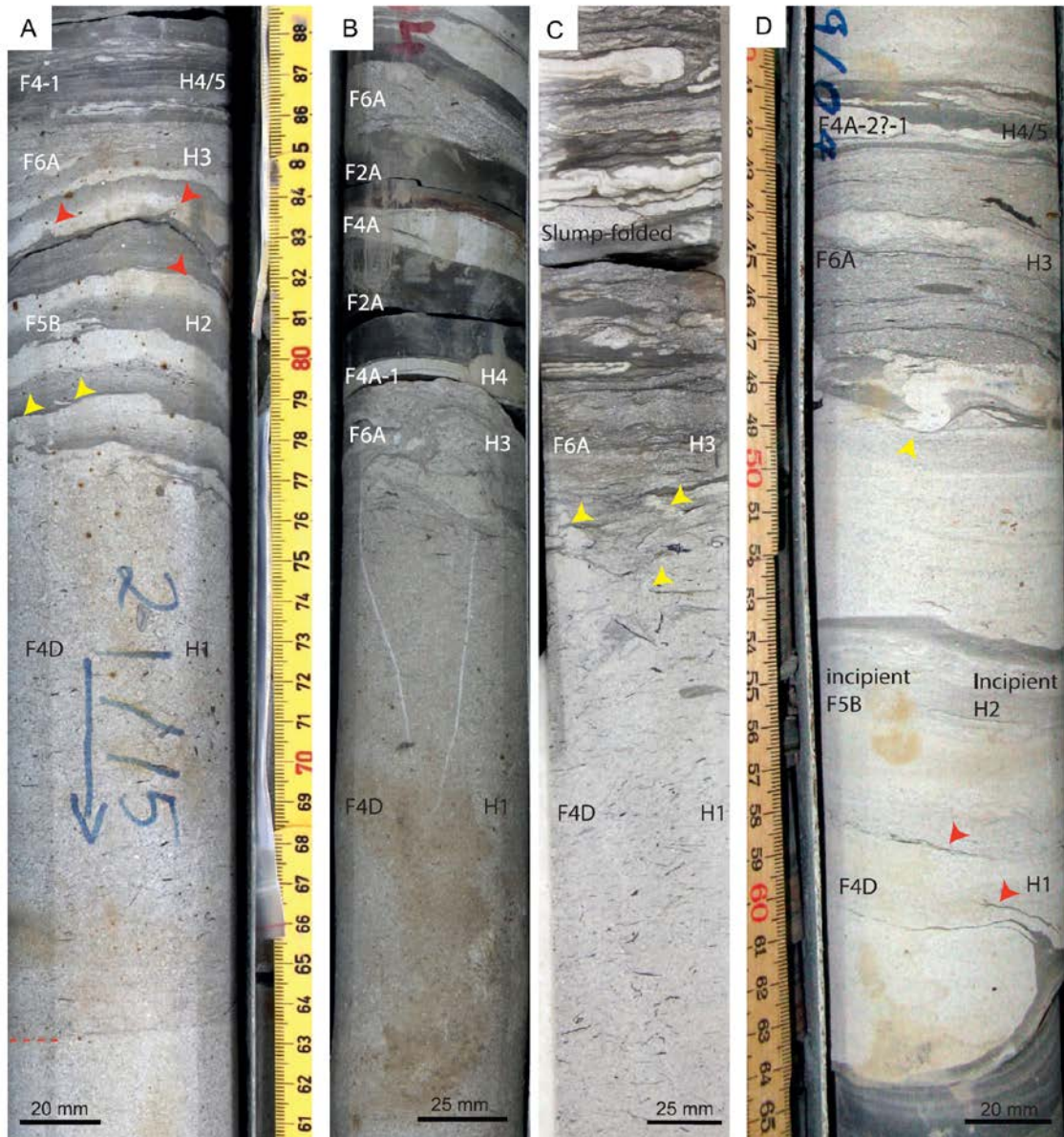


Figure 8. Examples of hybrid event beds. A) Top part of an approximately 25-cm-thick structureless sandstone (F4D; H1) overlain by an interval of banded sandstone–muddy sandstone (F5B; H2), and further thin tabular unit comprising muddy sandstone (F6A; H3). In the top, H3 is sharply overlain by millimeter-scale heterolithic interlamination showing local pseudonodular siltstone lenses (H4–5). Yellow arrows, water escape structures; red arrows, flame structures and mudstone injections; dashed red line, intra H1 boundary recording abrupt increase in organic-matter fragments. B) Top part of an approximately 22-cm-thick structureless sandstone

(H1) overlain by chaotic muddy sandstone (H3), and ripple cross-laminated fine-grained sandstone topped by millimeter-scale clay drape (H4–H5). Top of the figure shows interbedded structureless clayey mudstone beds (fluid mud), ripple cross-laminated sandstone, and muddy sandstone (debrite) beds. C) Top of an approximately 25-cm-thick structureless sandstone (H1) overlain by a chaotic muddy sandstone interval (H3). The muddy sandstone is slump folded and mixed with well-sorted sandstone facies. D) Small-scale example of a hybrid bed. Flame structures are horizontally oriented (sheared?) and may follow the base of incipient banding (red arrow). From Hovikoski et al. (2016)

4.4. Source Rock Screening and Biomarker analyses

A comprehensive analytical program of source rock screening analyses are concluded by GEUS and VPI, amounting in total to approx. 340 samples (Petersen 2013; VPI 2012a; Petersen et al. 2014). These data clearly identified an immature oil prone lacustrine mudstone succession of excellent quality with a minimum thickness exceeding 500+ meter as neither the base nor the top of the succession was identified. Approximately a half of the 500 m cored section is estimated to be composed by organic rich mudstones with average TOC and HI values of 2.88% and 5.66 mgHC/gTOC, respectively, thus demonstrating a highly oil-prone source rocks world-class source rock interval dominated by Type I and Type I/II kerogen (Fig. 9). The generative potential and significance of the source rock succession is discussed in detailed in Petersen et al. 2014.

In addition to the standard source rock screening data, it was decided to supplement with detailed analyses of the biomarker composition. The aims of these analyses were multiple: i) to provide input on the character of the organic component of the lake succession (land-plant material vs lacustrine algae vs marine indications), ii) to investigate the thermal maturity, iii) to identify biomarkers sensitive to thermal gradients over narrow intervals (500 m) in immature sections, and iii) investigate for new unknown components. The results will be described and documented in another technical note, but may be summarized as documenting that the lake was anoxic with significant bacterial activity in the water column which degraded the by far dominating lacustrine algae matter (Nytoft et al 2015).

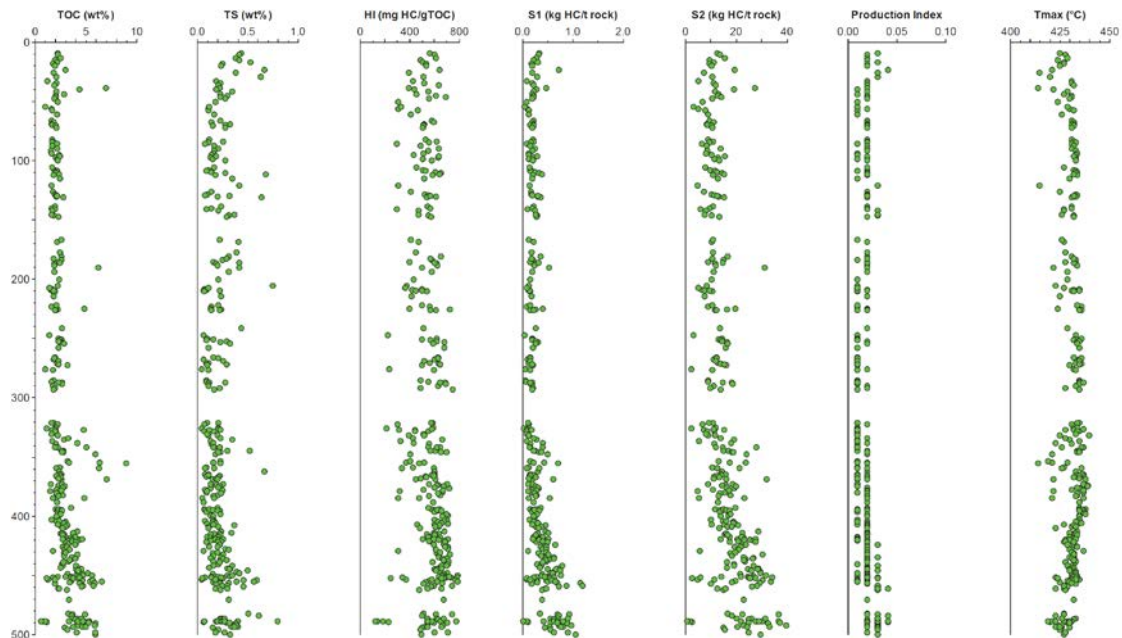


Figure 9. Geochemical source rock screening data, ENRECA-3 well. From Petersen et al., 2014.

4.5. Porosity and permeability of potential carrier beds

The interbedded nature of the potential source rocks and the sandy density flow beds may potential form a very effective drainage system for generated hydrocarbons facilitating the expulsion and migration. Therefore the potential carrier beds were assessed by estimating the thickness, grainsize and porosity and permeability of selected beds.

In order to investigate the quality of the potential carrier beds, 24 sandstone samples were selected for determination of helium (gas) porosity, grain-size and density, and Klinkenberg permeability. The porosity ranges from 10.2–20.8 %, while the Klinkenberg permeability ranges from less than 1 to 40 mD showing a distinct correlation with the grain-sizes that ranges from very fine to medium grained. The grain density is typically 2.6 g/cm³. The low permeability is interpreted as a result of poor connectivity between the pores (VPI 2012c).

4.6. Petrography

The analyses of sandstone petrography were performed on 10 representative samples from the thick relatively clean turbidite beds from which the grain-size distribution was determined in thin sections (VPI 2012b). The mineralogical composition of the sandstones

classify them as arkoses. The grain-size of the sandstones varies from fine to medium, being most commonly medium grained. The grain sorting is mostly poor and moderate to good. The visible porosity of the studied sandstone is very good. The visible pores consist mostly of well preserved primary pores partly enhanced by secondary pores due to dissolution of unstable grains. The pore interconnectivity is partly reduced due to various cement phases and compaction. The grains are commonly angular and sub-angular to sub-rounded with few rounded. Grain contacts are mainly point to point and floating type indicating weak to moderate compaction.

The clay fraction was analyzed by X-Ray Diffractometry (XRD) in 10 samples. The results show that the clay minerals are mainly composed of illite, kaolinite and subordinate amount of chlorite, smectite and mixed layer clay of illite–smectite (VPI 2012b).

5. Discussion – implications, hypotheses and future studies

5.1. Depositional evolution and sedimentary facies

As mentioned above, the completed sedimentological work has mainly dealt with process sedimentology of the gravity flow facies. The results have the following implications for petroleum geology:

- 1) The observation of common lacustrine hybrid beds contributes to exploration models in rift-lake systems. Cohesive debrites, such as those associated with hybrid beds, are in general characterized by low permeability and can thus form flow barriers in hydrocarbon reservoirs. Most of the debrite intervals in the studied hybrid beds are thin, assigned to late-stage flow concentration and thus can be expected to pinch out up-dip.
- 2) Collectively, the data point to short sediment transport distances and an immature sand source(s), low event frequency, and locally very limited clastic sedimentation between event deposition. In practice, this means that sandstone facies occur in direct communication with source rock facies and that similar facies may act as reservoirs/carrier beds in analogous deeply buried deposits. Moreover, these data tentatively suggest that the density flows were mainly associated with aprons and/or small deltas, whereas basin-floor fans attached to larger river systems have not been identified from the studied in lake system. This interpretation requires further testing during the PEXMOD study (see below).

The PEXMOD study builds on the accomplished work and will concentrate to improve understanding of stratigraphic evolution of the lake successions (lake phases and facies associations) and source rock accumulation controlling factors. The study also aims to get insights into sandstone source(s) (e.g., axial deltas vs. transverse aprons and fan deltas) and thereby to architecture of sandstone units. The approach will be multidisciplinary where sedimentological data such as mud-rock sedimentology and documentation of parasequence styles of gravity flow successions are combined with organic geochemistry, anoxia and climate proxy data derived from XRF analyses, as well as outcrop data from Bach Long Vi Island (C4).

5.2. Sandstone Petrography

The available petrographic data point to a local, relatively immature sediment source. The PEXMOD working group will consider if a petrographic study of selected and variable density flow beds, i.e. high density turbidites, low-density turbidites, debrites, and hybrid event beds is feasible in order to investigate if they have a common source area (e.g., rift-shoulder origin vs. long distance axial).

Moreover, a number of samples shall be collected for petrography and detrital zircon analyses from neighboring wells to investigate if the ENRECA-3 sandstones have similar hinterland and source areas as sandstones encountered in other well-sections in the north-eastern Song Hong Basin. Thus it is proposed to collect samples from the Oligocene succession in selected wells in the blocks 101, 106, 107 to be included in the PEXMOD study. These analyses are expected to provide input for assessments of the sediment transport routes and entry points, and also the mineralogical maturity and thus poro-perm of potential Oligocene reservoirs.

5.3. Poro-perm analyses

The data analyzed suggest that the sandstone interbeds hold variable reservoir/carrier bed potential, locally with reduced permeability. In the PEXMOD study it will be considered if is feasible to investigate the theme further. This could include a detailed study of the vertical development of poro-perm within some selected flow beds such as the thick sandstone turbidites vs. the debrite-bearing hybrid event beds.

5.4. Structural-Depositional model

Due to Neogene inversion of the Bach Long Vi Graben, the original Oligocene graben outline and sediment source areas are not precisely known. Nevertheless, the seismic data are suggestive of a narrow basin outline (more than ~ 10 km wide) with the graben being confined by active Paleogene faults on both sides of the lake. As mentioned above several lines of evidence tentatively suggest that the event sedimentation described here was generated by successive collapses triggered by tectonic instability in the syn-rift lake.

The Pexmod project will study the subject and aims to get insights to the role of tectonic and structural control on sedimentation.

5.5. Implications for exploration

The Enreca-3 core represents a unique window to deep lake deposition along the flanks of the Song Hong Basin during the rift climax phase. The data indicate that several hundreds of meters thick highly oil-prone petroleum source rock successions exist in the area and that source rock facies can be directly interbedded with thin sandstone successions potentially assisting oil expulsion. In the PEXMOD project, the data derived from the core will be extrapolated to comparable successions elsewhere in the northern Song Hong Basin, where core data are not available. The ENRECA-3 core section is interpreted to have formed during rift climax in the Bach Long Vi Graben, allowing the establishment of a deep lake due to the outpace of subsidence relative to sedimentation. Similar rift-climax sections will be identified in adjacent areas based on seismic sections and well data, which will be done in an attempt to predict the gross depositional outline of the Oligocene in these areas, and thereby contribute to the prediction of source- and reservoir rock intervals. Predicting reservoir and source rock intervals are fundamental to exploration and can therefore help formulating a predictive exploration model.

6. Conclusions

Existing analyses document that the ENRECA-3 well cored a highly oil-prone lacustrine setting. The entire succession has been tentatively assigned to the *Verrutricolporites pachydermus* sub-zone corresponding to a Late Oligocene age of the sediments. The lake session is composed by organic rich pelagic mudstones, which are interbedded with sand and mud gravity flow units. The sandstone intervals are composed by fine to medium-grained, subrounded to angular arcossic sand with porosities between 10.2 and 20.8 % and Klinkenberg permeability between less than 1 to 40 mD. The mudstones are composed by illite, kaolinite and subordinate amount of chlorite, smectite and mixed layer clay of illite–smectite. Highly oil-prone source rocks make up roughly half of the core section with TOC and HI averaging 2,88% and 566 mg HC/gTOC, respectively.

The data collected indicate that rich oil-prone source rock can develop at the margin of the Song Hong Basin under given conditions. The prerequisites include long-lived, protected deep lake setting generated by the rift-climax tectonics, which allow semi-permanent water column stratification and relatively sediment starved setting.

The Enreca-3 related studies have two main aims in the PEXMOD project: the first is to achieve a detailed understanding of the depositional evolution of the lake system and its key controls (e.g., tectonic vs. climatic). The main data set are XRF-based analyses and new sedimentological data. The results are expected to give insights into themes such as source rock accumulation controlling factors and reservoir architecture. Outcome of this work will include a tectonostratigraphic lake model.

Secondly, the Enreca-3 data will be put into regional exploration context. The ENRECA-3 core represents a unique window to deep lake deposition during the rift climax phase and the data can be extrapolated to tectonostratigraphically analogous successions.

7. Acknowledgement

Danida is thanked for financing the long-term ENRECA project; Danida and PetroVietnam are thanked for contributing to the funding of the coring of the ENRECA-3; VPI and GEUS are thanked for providing manpower and logistic support. PetroVietnam, VPI and GEUS are thanked for permission to report the results.

8. References

Andersen, C., Mathiesen, A., Nielsen, L.H., Tiem, P.V., Petersen, H.I, and Diem, P.T., 2005, Evaluation of petroleum systems in the northern part of the Cainozoic Song Hong Basin (Gulf of Tonkin), Vietnam: *Journal of Petroleum Geology*, v. 28, p. 167–184.

Bohacs, K. M., Carroll, A. R., Neal, J. E., and Mankiewicz, P. J., 2000, Lake-basin type, source potential, and hydrocarbon character: an integrated sequence-stratigraphic-geochemical framework. In: Gierlowski-Kordesch, E. H. and Kelts, K. R. (eds.), *Lake basins through space and time*. AAPG Stud. Geol. 46, p. 3–34.

Fyhn, M.B.W., and P.V. Phach, 2015, Late Neogene structural inversion around the northern Gulf of Tonkin, Vietnam: Effects from right-lateral displacement across the Red River fault zone: *Tectonics*, v. 34, p. 290–312.

Gawthorpe, R.L. and Leeder, M.R., 2000, Tectono-sedimentary evolution of active extensional basins. *Basin Research*, v. 12, p. 195–218.

Huang, B., Tian, H., Wilkins, R.W.T., Xiao, X., and Li, L., 2013, Geochemical characteristics, palaeoenvironment and formation model of Eocene organic-rich shales in the Beibuwan Basin, South China Sea: *Marine and Petroleum Geology*, v. 48, p. 77–89, doi: 10.1016/j.marpetgeo.2013.07.012.

Katz, B. J., 1995, A survey of rift basin source rocks, in Lambiase, J. J. (ed.), *Hydrocarbon habitat in rift basins: The Geological Society Special Publication 80*, p. 213–242.

Lambiase, J., 1990, A model for tectonic control of lacustrine stratigraphic sequences in continental rift basins. In “*Lacustrine basin exploration - case studies and modern analogs*”. Association of Petroleum Geologists Memoir 50, p. 265–276.

Lambiase, J., and Bosworth, W., 1995.-Structural controls on sedimentation in continental rifts. In: J.J. LAMBIASE (ed.), *Hydrocarbon Habitat in Rift Basins*. Special Publications-Geological Society of London 80, p. 117–144.

Leloup, P.H., R. Lacassin, P. Tapponnier, U. Schärer, Z. Dalai, L. Xiaohan, Z. Liangshang, J. Shaocheng, and P.T. Trinh, 1995, The ASRR shear zone (Yunnan, China), Tertiary transform boundary of Indochina: *Tectonophysics*, v. 251, p. 3–84.

Liu, E., Wang, H. Li, Y., Zhou, W., Leonard, N.D., and Lin, Z., 2014, Sedimentary characteristics and tectonic setting of sublacustrine fans in a half-graben rift depression, Beibuwan

Basin, South China Sea: *Marine and Petroleum Geology*, v. 52, p. 9–21, doi.: 10.1016/j.marpetgeo.2014.01.008.

Nielsen, L.H., 2013, Preliminary report on the sedimentary facies of the Enreca-3 core and further analytical results. Geus report 2013/55.

Nielsen, L.H., Fyhn, M.B.W., Petersen, H.I., Hovikoski, J., Therkelsen, J., Tuan, H.A., Oanh, N.K., Minh, N.H., Tan, H.M., Phuong, B.T.N., Thang, P.V., Quang, C.D., and Abatzis, I., 2014, Stratigraphic Core Wells Enreca-1, -2 And -3: Results Of The Song Ba Rift, Phu Quoc Island And Bach Long Vi Island Drilling Campaigns. *PetroVietnam Journal*, v. 10, p. 30–38.

Nøttvedt, A., Gabrielsen, R. H., and Steel, R. J., 1995, Tectonostratigraphy and sedimentary architecture of rift basins, with reference to the northern North Sea: *Marine and Petroleum Geology*, v. 8, p. 881–901.

Nytoft, H.P., Petersen, H.I., Fyhn, M.B.W., Nielsen, L.H., Hovikoski, J., and Abatzis, I., 2015, Novel saturated hexacyclic C34 and C35 hopanes in lacustrine oils and source rocks: *Organic Geochemistry*, v. 87, p. 107–118.

Petersen, H.I., 2013, Source rock evaluation of the Enreca-3 well; Bach Long Vi Island, Song Hong Basin, Vietnam. Geus report 2013/16.

Petersen, H.I., Fyhn, M.B.W., Nielsen, L.H., Tuan, H.A., Quang, C.D., Tuyen, N.T., Thang, P.V., Tham, N.T., Oang, N.K., and Abatzis, I., 2014, World-class Paleogene oil-prone source rocks from a cored lacustrine syn-rift succession, Bach Long Vi Island, Song Hong Basin, offshore northern Vietnam: *Journal of Petroleum Geology*, v. 37, p. 373–389.

Prosser, S., 1993, Rift-related linked depositional systems and their seismic expression, in G. D. Woudjams and A. Dobb, (eds.), *Tectonics and seismic sequence stratigraphy: Geological Society Special Publication 71*, p. 35–66.

Rangin C., M. Klein, D. Roques, X.L. Pichon, L.V. Trong, The Red River fault system in the Tonkin Gulf, Vietnam: *Tectonophysics*, v. 243, p. 209–222.

Sladen, C., 1997, Exploring the lake basins of East and Southeast Asia. In “*Petroleum Geology of Southeast Asia*”. Geological Society, London, Special Publications, 126, p. 49–76.

Tapponnier, P., Peltzer, G., and Armijo, R., 1986, On the mechanics of the collision between India and Asia, in M.P. Coward A.C. Ries (eds.), *Collision Tectonics*, Geological Society, London, Special Publications 19, pp. 115–157.

Todd, S. P., Dunn, M. E. and Barwise, A. J. G., 1997. Characterizing petroleum charge systems in the Tertiary of SE Asia. In: Fraser, A. J. Matthews, S. J. and Murphy, R. W. (eds.), Petroleum geology of Southeast Asia. Geol. Soc. London Spec. Publ. 126, 25–47.

VPI, 2012a, Geochemical analysis. Sample analysis report, Enreca-3 core.

VPI, 2012b, Petrography and XRD analyses study of interval 18.30m-499.68m. Petrography report, Enreca-3 core.

VPI, 2012c, Routine core analyses. Core analysis report, Enreca-3 core.

VPI, 2013, Biostratigraphy report, Enreca-3 core.

Williams, H. H., Fowler, M. and Eubank, R. T., 1995. Characteristics of selected Palaeogene and Cretaceous lacustrine source rocks of Southeast Asia. In: Lambiase, J. J. (ed.), Hydrocarbon habitat in rift basins. Geol. Soc. London Spec. Publ. 80, 241–282.

9. Appendix A: Core Photos



ENRECA-3 Core, Boxes 1 & 2, Interval 0,7-10m



ENRECA-3 Core, Boxes 3 & 4, Interval 10-20 m



ENRECA-3 Core, Boxes 5 & 6, Interval 20-30 m



ENRECA-3 Core, Boxes 7 & 8, Interval 30-40 m



ENRECA-3 Core, Boxes 9 & 10, Interval 40-50 m



ENRECA-3 Core, Boxes 11 & 12, Interval 50-60 m



ENRECA-3 Core, Boxes 13 & 14, Interval 60-70 m



ENRECA-3 Core, Boxes 15 & 16, Interval 70-80 m



ENRECA-3 Core, Boxes 17 & 18, Interval 80-90 m



ENRECA-3 Core, Boxes 19 & 20, Interval 90-100 m



ENRECA-3 Core, Boxes 25 & 26, Interval 120-130 m



ENRECA-3 Core, Boxes 27 & 28, Interval 130-140 m



ENRECA-3 Core, Boxes 29 & 30, Interval 140-150 m



ENRECA-3 Core, Boxes 31 & 32, Interval 150-160 m



ENRECA-3 Core, Boxes 33 & 34, Interval 160-170 m



ENRECA-3 Core, Boxes 35 & 36, Interval 170-180 m



ENRECA-3 Core, Boxes 37 & 38, Interval 180-190 m



ENRECA-3 Core, Boxes 39 & 40, Interval 190-200 m



ENRECA-3 Core, Boxes 41 & 42, Interval 200-210 m



ENRECA-3 Core, Boxes 43 & 44, Interval 210-220 m



ENRECA-3 Core, Boxes 45 & 46, Interval 220-230 m



ENRECA-3 Core, Boxes 47 & 48, Interval 230-240 m



ENRECA-3 Core, Boxes 49 & 50, Interval 240-250 m



ENRECA-3 Core, Boxes 51 & 52, Interval 250-260 m



ENRECA-3 Core, Boxes 53 & 54, Interval 260-270 m



ENRECA-3 Core, Boxes 55 & 56, Interval 270-280 m



ENRECA-3 Core, Boxes 57 & 58, Interval 280-290 m



ENRECA-3 Core, Boxes 59 & 60, Interval 290-300 m



ENRECA-3 Core, Boxes 61 & 62, Interval 300-310 m



ENRECA-3 Core, Boxes 63 & 64, Interval 310-320 m



ENRECA-3 Core, Boxes 65 & 66, Interval 320-330 m



ENRECA-3 Core, Boxes 67 & 68, Interval 330-340 m



ENRECA-3 Core, Boxes 69 & 70, Interval 340-350 m



ENRECA-3 Core, Boxes 71 & 72, Interval 350-360 m



ENRECA-3 Core, Boxes 73 & 74, Interval 360-370 m



ENRECA-3 Core, Boxes 75 & 76, Interval 370-380 m



ENRECA-3 Core, Boxes 77 & 78, Interval 380-390 m



ENRECA-3 Core, Boxes 79 & 80, Interval 390-400 m



ENRECA-3 Core, Boxes 81 & 82, Interval 400-410 m



ENRECA-3 Core, Boxes 83 & 84, Interval 410-420 m



ENRECA-3 Core, Boxes 85 & 86, Interval 420-430 m



ENRECA-3 Core, Boxes 87 & 88, Interval 430-440 m



ENRECA-3 Core, Box 89, Interval 440-445 m



ENRECA-3 Core, Boxes 90 & 91, Interval 445-455 m



ENRECA-3 Core, Boxes 92 & 93, Interval 455-465 m



ENRECA-3 Core, Boxes 94 & 95, Interval 465-475 m



ENRECA-3 Core, Box 96, Interval 475-480 m

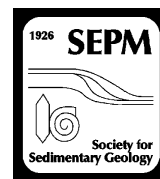


ENRECA-3 Core, Boxes 97 & 98, Interval 480-490 m



ENRECA-3 Core, Boxes 99 & 100, Interval 490-500 m

10. Appendix B: Hovikoski et al. (2016)



DENSITY-FLOW DEPOSITION IN A FRESH-WATER LACUSTRINE RIFT BASIN, PALEOGENE BACH LONG VI GRABEN, VIETNAM

JUSSI HOVIKOSKI,¹ JENS THERKELSEN,¹ LARS H. NIELSEN,¹ JØRGEN A. BOJESEN-KOEFOED,¹ HANS P. NYTOFT,¹ HENRIK I. PETERSEN,² IOANNIS ABATZIS,¹ HOANG A. TUAN,³ BUI THI NGOC PHUONG,⁴ CAO VAN DAO,⁴ AND MICHAEL B.W. FYHN¹

Geological Survey of Denmark and Greenland (GEUS), Øster Voldgade 10, 1350 Copenhagen, Denmark

Maersk Oil, Esplanaden 50, DK-1263 Copenhagen K, Denmark

Petroleum Exploration Division, Vietnam Oil and Gas Group (PETROVIETNAM), 18 LangHa Street, Ba Dinh District, Hanoi, Vietnam

VPI_Labs, Vietnam Petroleum Institute, Block G1, Thanh Da Hotel, 27 Ward, Binh Thanh District, Ho Chi Minh City, Vietnam

e-mail: jhov@geus.dk

ABSTRACT: The aim of this study is to describe density-flow facies variability and interpret their flow evolution in a fresh-water rift-lake system. The data were collected from the 500-m-thick Paleogene lacustrine oil-prone source-rock succession penetrated by the Enreca-3 core-hole at the intersection of the Song Hong and the Beibuwan basins, Vietnam. The sedimentological data collected are supplemented with source-rock screening data to get an insight into the origin of mud in the density flows. A wide range of density-flow facies are recognized and can be assigned to turbulent, transitional, and laminar flow processes. The beds range from centimeter-scale, mudstone-rich beds to meter-scale cohesive debrites and hybrid beds. Similarly to the “classic” hybrid beds, the centimeter-scale beds are interpreted to record flow transformation and concentration. The hybrid bed motifs include essentially similar bed divisions (H1–H5; Haughton et al. 2009) to those described from marine basins. Moreover, transitional-flow facies are particularly common and include transitional current ripples and variously developed cyclic banding and lamination. These facies occupy a fixed position below and/or at plug-flow units in the bed motifs, suggesting that flow dynamics related to plug-flow development governed their development. Source-rock screening data show that most of the mudstone in hybrid beds represents lake-bottom and lake-margin mud, which was likely assimilated into the density flows along their path. Similarly, sedimentological data show common evidence for interaction between flow and the muddy lake floor such as sheared flame structures, deformed mud intrusions, and interbeds in turbidite facies. The assimilation of the lake-bottom mud into the density flows probably played a key role in modulating flow turbulence and explains the common occurrence of transitional-flow facies and indications of late-stage flow concentration in these strata.

INTRODUCTION

Hybrid beds—deposits showing change in flow type from turbidity current to debris flow during a single flow event—are described from a number of marine basin-floor depositional systems (e.g., Lowe and Guy 2000; Lowe et al. 2003; Haughton et al. 2003; Talling et al. 2004; Amy and Talling 2006; Barker et al. 2008; Haughton et al. 2009; Hodgson 2009; Sumner et al. 2012; Talling et al. 2012a; Talling 2013; Patacci et al. 2014). They are particularly common in many distal fan settings (e.g., Haughton et al. 2009; Talling 2013 and references therein), but they have been also reported from more proximal positions near confining topography (Patacci et al. 2014), avulsion splays (Power et al. 2013; Terlaky and Arnott 2014), or even channels (Sylvester and Lowe 2004). Hybrid beds may form in various ways, but they are generally thought to form as a result of longitudinal changes in the flow rheology of a passing density flow. A key factor in flow transformation and concentration is incorporation of mud into the density flow. Depending on the flow velocity, even a relatively minor increase in clay content can modulate the turbulence and/or transform the turbidity current into a nearly laminar flow (Baas et al. 2009; Sumner et al. 2009; Baas et al. 2011; Talling et al. 2012b; Talling 2013).

Previous models have postulated that the mud can be derived from the original failure at the start of the event, or is subsequently incorporated into the flow by seafloor erosion. Haughton et al. (2009) suggested that particularly the latter can be a central process in the formation of hybrid beds in many cases. This inference has been recently supported by laboratory experiments (e.g., Verhagen et al. 2013), but validating evidence from the rock record (see e.g., Ito 2008) is still rare.

Recent flume-tank studies have greatly increased our ability to interpret flow processes from ancient clay-rich density-flow deposits (e.g., Baas and Best 2002; Ilstad et al. 2004; Schieber et al. 2007; Baas et al. 2009; Sumner et al. 2009 and Baas et al. 2011). Baas et al. (2009, 2011) recognized that most clay-rich decelerating flows evolve through five flow phases: turbulent flow, turbulence-enhanced transitional flow, lower and upper transitional plug flow, and quasi-laminar plug flow. However, to date there have been limited attempts to apply these insights to the rock record (see e.g., Mackay and Dalrymple 2011; Kane and Ponten 2012; Stevenson et al. 2014 for exceptions).

Although fluid muds (fine-grained sediment suspension with a solid concentration more than 10 g L⁻¹) have been documented from freshwater

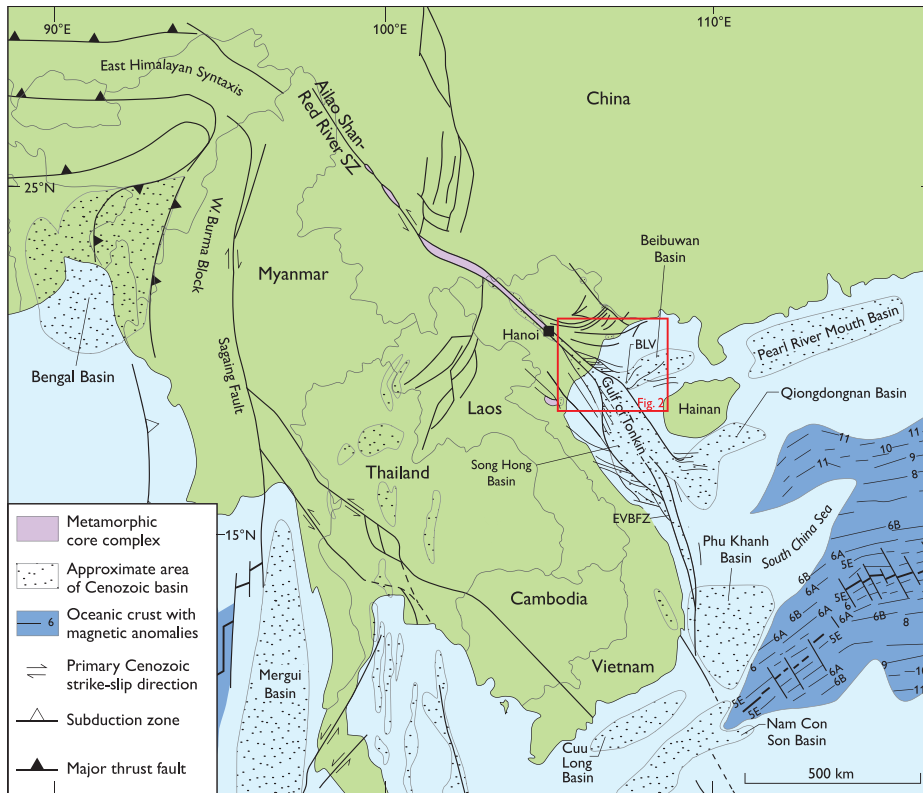


FIG. 1.—Simplified structural outline of Cenozoic basins and selected fault zones onshore and offshore Indochina and southernmost China, modified after Fyhn and Phach (2015) and references therein. Box indicates the location of Figure 2. BLV, Bach Long Vi Island; EVBFZ, East Vietnam Boundary Fault Zone.

systems (McAnally et al. 2007), and deposits similar to hybrid beds have been formed experimentally in flume-tank studies using fresh water (e.g., Sumner et al. 2009; Baas et al. 2011), hybrid beds have not been reported from freshwater lacustrine basins so far. The general rarity of gravity-flow studies from freshwater basins is unfortunate, since the near lack of endobenthic bioturbation in such settings increases the preservation potential particularly of small-scale, mud-dominated density-flow events, in which flow behavior can be recorded on millimeter scales (e.g., Schieber et al. 2007; Macquaker et al. 2010; Mackay and Dalrymple 2011). Deep lacustrine basins may also host petroleum source rocks; screening data that reveal the organic-matter type in the mudstone facies can offer important information regarding the origin of the mud in the density-flow beds (e.g., extrabasinal vs. intrabasinal lake-floor mud). Consequently, deep lacustrine basins can be well-suited settings for detailed studies of density-flow processes and their sedimentary facies.

In comparison to many marine basins, deep lake systems can be more commonly prone to water-rich muddy basin floors. McAnally et al. (2007) reported that many eutrophic lake bottoms are anoxic and characterized by bottom-hugging fluid-mud suspensions, where high organic-matter content hinders consolidation. A growing body of literature suggests that such fluid-rich substrates can readily interact with overriding density flows (Verhagen et al. 2013; Baas et al. 2014; Butler et al. 2016), and promote flow concentration by assimilation of the lake-bottom mud into the density-flow body. If the density flow is initially turbulent, assimilation of mud will probably modulate the turbulence and transform the flow to transitional and/or to laminar as the flow decelerates. This could be especially the case in deep, tectonically active lake systems such as rift lakes where episodic collapse-triggered density flow can be expected to be an important sediment delivery mechanism and the lake floor is commonly anoxic allowing preservation of organic matter. Therefore, hypothetically, eutrophic rift lakes can promote development of hybrid beds via lake-floor erosion and transitional-flow deposits can be particularly well expressed.

The 500-m-long Enreca-3 core, Vietnam, penetrates a Paleogene, freshwater rift-lake system that is characterized by a range of density-flow beds, which are interbedded with oil-prone source-rock mudstones (Petersen et al. 2014). The deposits consist of debrites, hybrid beds (H1–H5; Haughton et al. 2009) and centimeter-scale mud-rich beds that largely deviate from the standard hybrid-bed model, but probably reflect similar flow transformation from turbulent to nearly laminar sedimentation during a flow event. This study aims to describe the main variability in density-flow beds recorded in the core, and attempts to compare the facies evolution of single beds with the flow phase diagram of Baas et al. (2009, 2011). Moreover, the sedimentological data collected are supplemented with strategic source-rock screening data from selected hybrid-bed units in order to get an insight into how flow transformation and concentration develop, and to test the postulated models for development of hybrid beds (see e.g., Haughton et al. 2009; Talling 2013).

MATERIAL AND METHODS

Geological Setting and Previous Studies

Bach Long Vi Island denotes the crest of the inverted Bach Long Vi Graben (Figs. 1, 2A). The graben formed during Eocene–Oligocene rifting in the Gulf of Tonkin area, linked with left-lateral faulting across the Ailao Shan–Red River Shear Zone, which led to the establishment of the Song Hong and the Beibuwan basins (Fyhn, in review). The Bach Long Vi Graben connects the Beibuwan Basin and the northeastern Song Hong Basin (Fig. 2B). The graben is roughly 10 km wide at its narrowest point, but farther north it merges with the Tra Co Graben and its width increases to more than 30 km. Seismic data and wells show that Paleogene highs mostly have upper Paleozoic carbonates in their cores, and Paleozoic–Mesozoic clastic deposits flank the grabens. The Bach Long Vi Graben was confined in between two such highs situated only few kilometers east and west of the present location of the Bach Long Vi Island, respectively

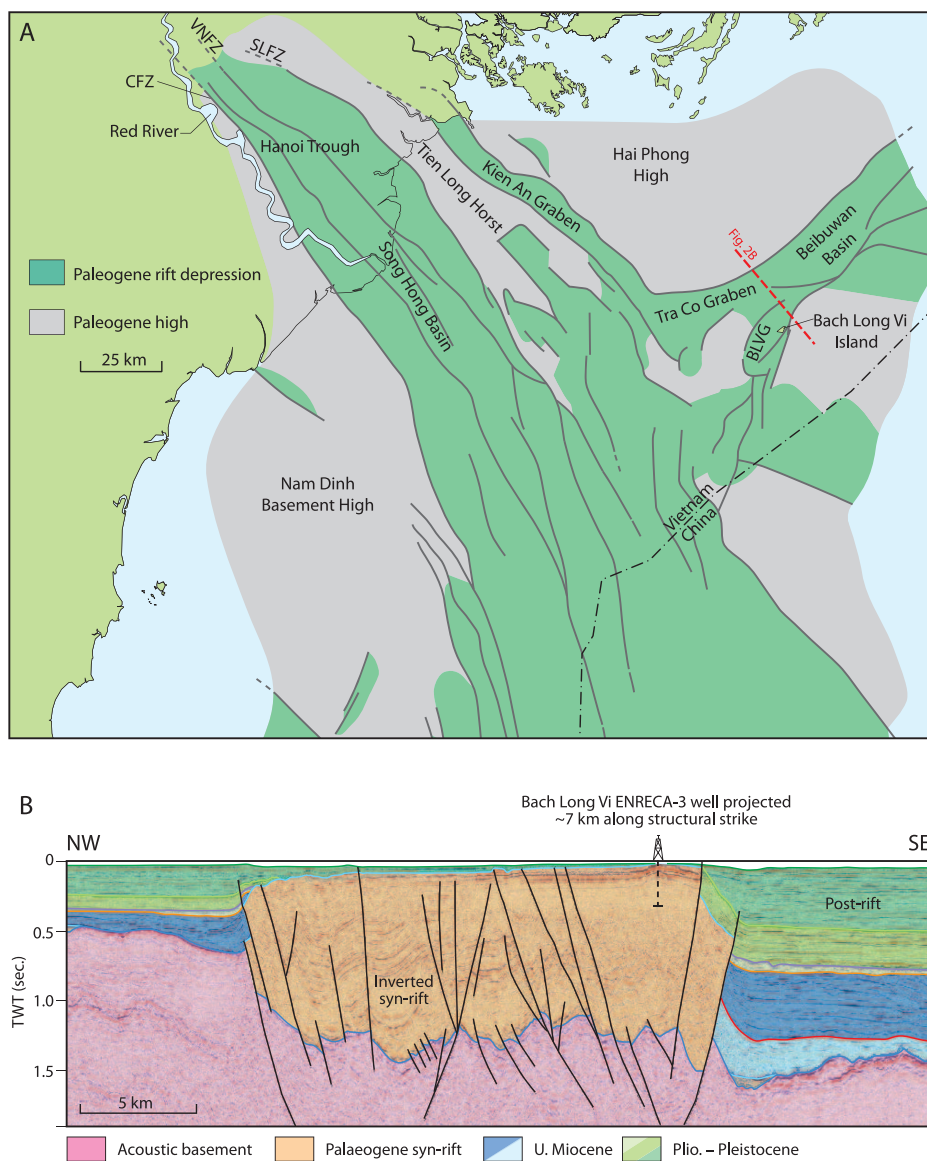


FIG. 2.—**A**) Structural outline of the northern Song Hong Basin and the western Beibuwan Basin emphasizing the main Paleogene faults, rift depressions, and structural highs. Bold red line indicates the position of Part B. BLVG, Bach long Vi Graben; CFZ, Chay Fault Zone; SLFZ, Song Lo Fault Zone; VNFZ, Vinh Ninh Fault Zone. **B**) Seismic transect across the Bach Long Vi inversion trend. The Paleogene graben underlying the Bach Long Vi Island has been strongly inverted throughout the Neogene. The ENRECA-3 core well drilled on the island is projected onto the transect. Location is shown in Part A.

(Fig. 2B). It is not clear whether these structural highs outlined hills during the Paleogene, but the lack of Paleogene strata burying these features could have resulted from a distinct relief of the graben flanks.

Vietnamese exploration wells drilled on the margin of the Song Hong Basin and in the Beibuwan Basin intersect thickly developed Paleogene rift-influenced fluvial and lacustrine deposits ranging from lake mudstones and lacustrine deltaic sandstones to alluvial conglomerates. A comparable depositional pattern is reported from the Chinese part of the Beibuwan Basin, where thick, organic-rich lacustrine mudstone intervals occur in the Liushagang Formation (Huang et al. 2013). The Paleogene syn-rift succession in the Chinese part of the basin is often attributed to the Paleocene–Oligocene. However, Fyhn (in review) argued for an Eocene–Oligocene age for the entire Beibuwan Basin comparable to other rift basins in the western South China Sea. The Eocene–Oligocene in the innermost of these basins are also dominated by nonmarine strata, and the cored succession investigated in this study thus provides a rare analogue to lacustrine syn-rift strata deeply buried along the South China Sea margin as well as elsewhere in SE Asia.

The stratigraphic ENRECA-3 well was drilled to investigate the depositional environment and the source-rock potential of the Paleogene lacustrine rift system, which constitutes the primary hydrocarbon play in the region (e.g., Nielsen et al. 1999; Andersen et al. 2005; Petersen et al. 2005). The well cored continuously 500 m of syn-rift sediments (Fig. 3). Previous studies dealing with the Enreca-3 core include the source-rock study by Petersen et al. (2014), which revealed the presence of a highly oil-prone source succession in the core. Other work relevant to the present paper includes the petrographic study by Phuong (2014), which included semi-quantitative XRD analyses on the clay fraction (< 2 μm) from 10 mudstone samples covering the whole Enreca-3 core. The analyses show that illite is the dominant clay mineral in all samples (< 63%), whereas kaolinite forms up to 31% of the clay fraction. Smectite, mixed layered illite–smectite, and chlorite occur in lower amounts (Phuong 2014). Moreover, previous studies have indicated that sedimentation took place under freshwater conditions. This is demonstrated by the presence of freshwater dinocysts, *Botryococcus* spp. and *Pediastrum* spp. algae, and low total sulfur content (Petersen et al. 2014).

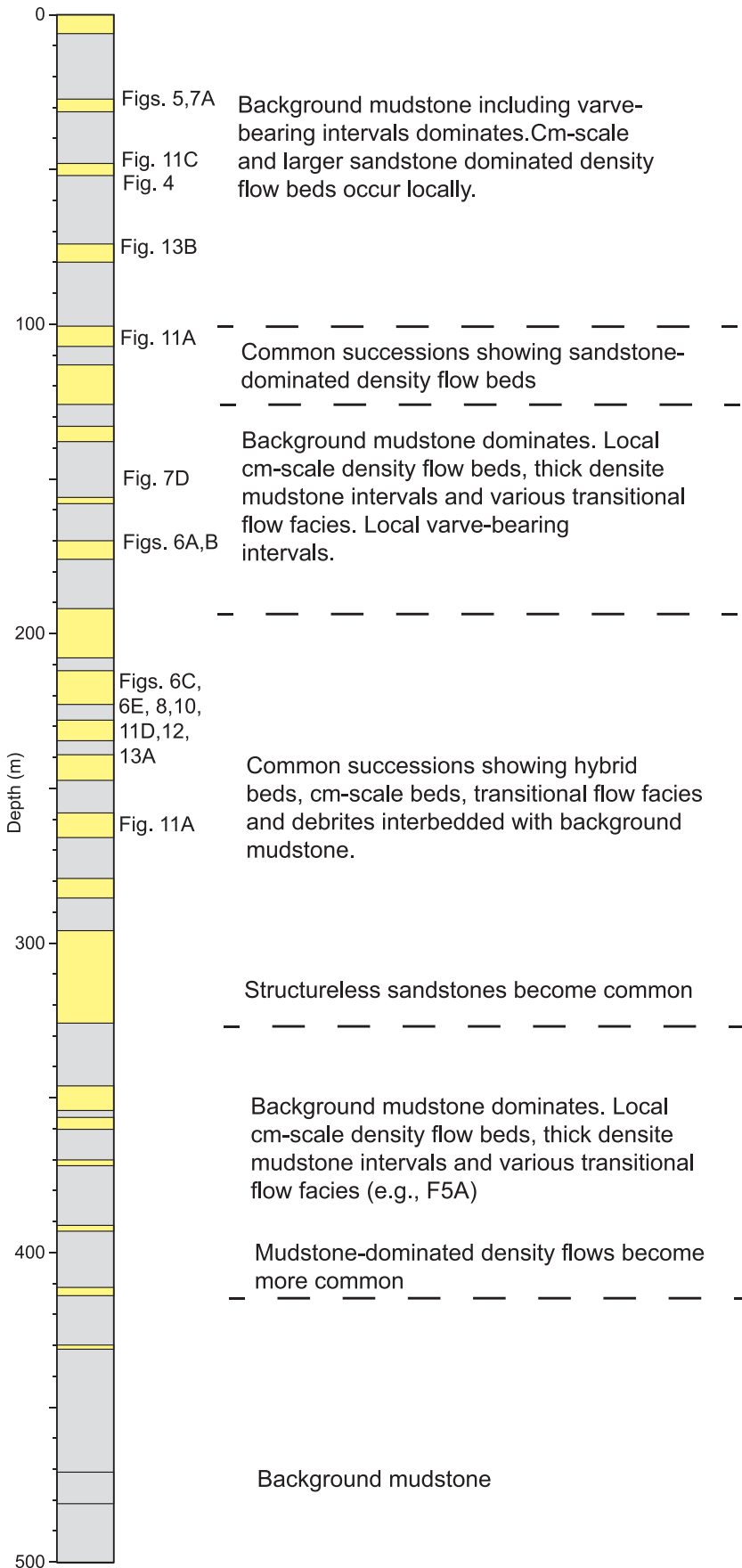


FIG. 3.—A simplified stratigraphic column of the Enreca-3 core.

TABLE 1.—Terminology for facies, hybrid beds, and debrites used in this study. A preliminary comparison to interpreted flow processes is also shown.

This Study	Flow Process (Baas et al. 2011)	Hybrid-Bed Division (Haughton et al. 2009)	Debrite Classification (Talling et al. 2009)	Other
F1A		H5 when associated with hybrid beds		Suspension settling
F1B				Hemipelagic settling
F2A	Upper Transitional Plug Flow (UTPF)		Fluid mud	
F2B	Incipient Quasi Laminar Plug Flow (QLPF)?		Incipient low-strength cohesive debrite?	
F3A	Sedimentation below TPF			
F3B	Lower Transitional Plug Flow (LTPF)			
F4A	Turbulent Flow (TF)	H4 when associated with hybrid beds		Tbc or Tc of Bouma (1962)
F4B	Turbulence-Enhanced Transitional Flow (TETF) - LTPF			
F4C	Minor residual turbulence under TPF	H1 when associated with hybrid beds		Ta of Bouma (1962)
F4D				Mixing of water and debris flow at the head of the flow?
F4E				
F5A	TETF-UTPF			
F5B	TPF-lamina scale occurrences of low concentration QLPF	H2		
F6A	QLPF	H3	Low-strength cohesive debrite	
F6B	QLPF	H3 if associated with hybrid beds	Intermediate-strength cohesive debrite	

Methods

This study is based primarily on macroscopic sedimentological core descriptions of selected intervals prone to gravity-flow beds. These data were supplemented with polished thin sections ($n = 9$) of selected facies. The thin sections were examined with a conventional petrographic light microscope and in certain cases with a backscattered scanning electron microscope. Moreover, selected mudstone core slabs were inspected with a stereo zoom binocular microscope to get qualitative insight into the silt and sand content. The petrographic data of Phuong (2014) are included in sandstone facies descriptions.

Furthermore, source-rock screening data are used to investigate the origin of the organic matter in density-flow-related mudstones. In order to test variations in kerogen type and petroleum potential, a series ($n = 30$) of selected facies including mud clasts of debrites, fluid-mud layers, and a “hyperpycnite-like” structure, were subjected to TC/TOC/TS/Rock-Eval type organic geochemical screening analysis. Total carbon (TC, wt%), total organic carbon (TOC, wt%), and total sulfur (TS, wt%) were determined by combustion in a LECO CS-200 induction furnace. The TOC was determined after elimination of carbonate-bonded carbon by prolonged HCl treatment. The petroleum potential was determined by Rock-Eval-type pyrolysis using a source rock analyzer (SRA) instrument, calibrated against the IFP160000 standard to ensure correspondence to standard Rock-Eval data. Part of the data (15 samples) has been previously published in Petersen et al. (2014).

In this study, sedimentary units that can be assigned to specific flow processes are referred to as “facies” and “sub-facies,” even when they form part of a single bed (see e.g., Amy and Talling 2006). Although such units could have been assigned to “divisions” or “units” within a density-flow bed (e.g., Haughton et al. 2009), the facies approach is preferred here since the bed motifs are variable and some of the individual units can also occur alone. Moreover, due to the case-study nature of this study, erecting new bed motif divisions does not seem desirable. In the discussion of density-flow types, facies described in this study and well-established divisions of turbidites (Bouma 1962), hybrid beds (Haughton et al. 2009; Talling 2013), and cohesive debrite types (Talling et al. 2012b) are used interchangeably. The relationships between the different division terms, interpreted flow processes (Baas et al. 2011) and their abbreviations are shown in Table 1. “Cohesive debrite” means deposit of a debris flow in which amount of fine mud and thereby cohesive strength is enough to support sand grains (Talling 2013). The term “mudstone” refers to fine-grained sedimentary rock that contains > 50% clay- and silt-size particles.

RESULTS AND INTERPRETATION

The data are divided into two broad categories, the first being “mudstone-dominated density-flow deposits” characterized by centimeter-scale mudstone-rich beds, and the second “sandstone-dominated density-flow deposits,” which commonly form hybrid beds and debrites (Haughton et al. 2009; Talling 2013).

Mudstone-Dominated Density-Flow Deposits

Fine-grained density-flow deposits are randomly interbedded with background lacustrine facies (varves or oil-prone, black micro-laminated to structureless mudstone that lacks clear bed boundaries), or are stacked, and form a few meters to about 10 m-thick upward-coarsening successions together with the sandstone-dominated density-flow deposits (see below, Figs. 4, 5). The facies and sub-facies (Figs. 6–8) are described and interpreted in Table 2, and a summary of the main bed motifs and their inferred flow evolution is presented below.

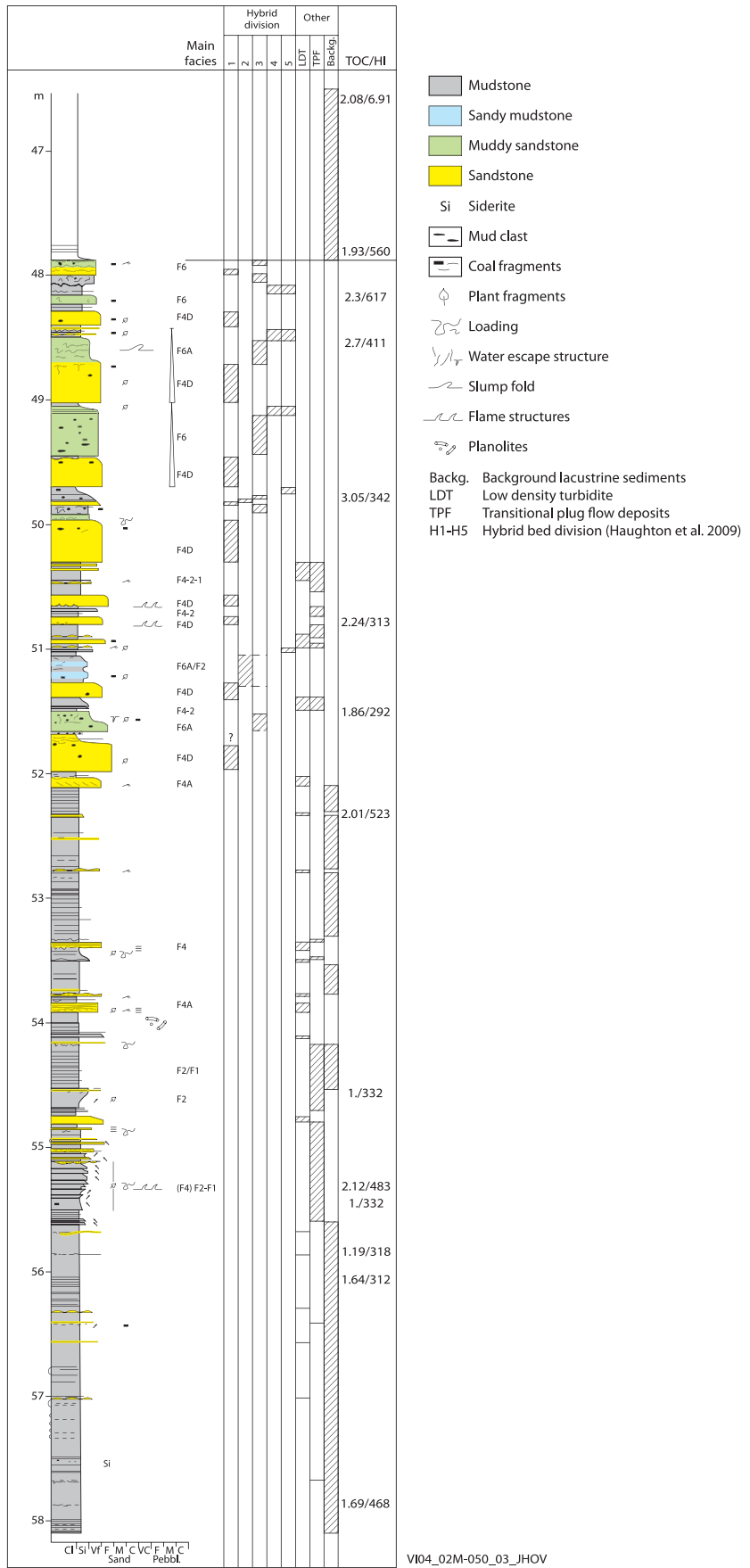


FIG. 4.—A sedimentological log illustrating an example of a meter-scale upward-coarsening parasequence typical of these deposits. Distribution of the main facies and corresponding hybrid-bed division or small-scale density-flow units are shown. Source-rock screening data (TOC/HI) are also presented.

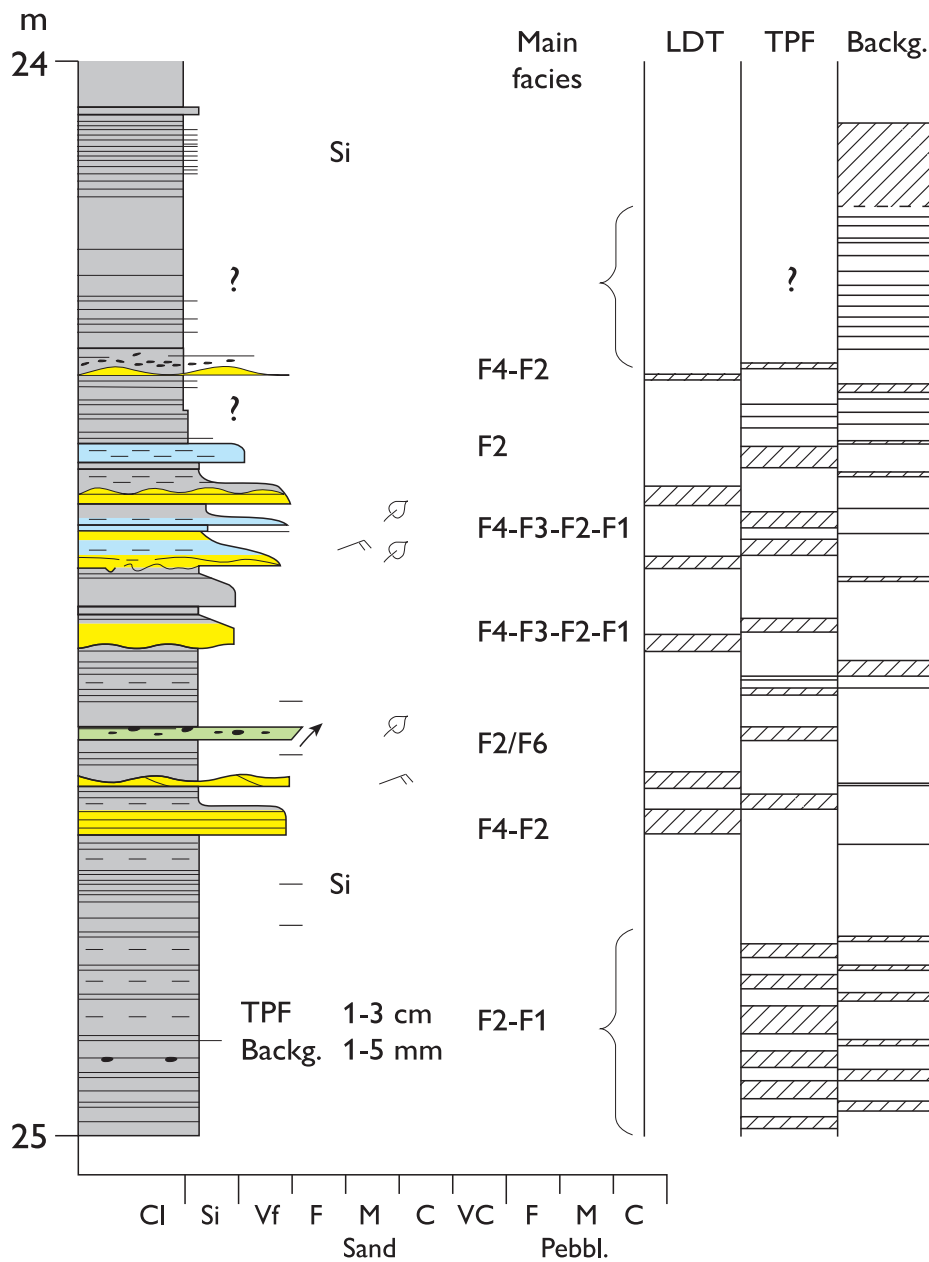


FIG. 5.—A detailed sedimentological log illustrating an example of alternating background hemipelagic lacustrine sediments interbedded with small-scale, mudstone-rich density-flow beds. Note that due to the thinness of the background deposits as well as masking concretionary processes (siderite), not all laminae can be illustrated, and the TPF-background interbedding is schematic. See Figure 3 for legend.

Motif 1: Low-Density-Turbidite-Based Bed (Fig. 9A).—The thickest and most complete beds contain four units:

- 1) A basal, flat-based parallel-laminated and/or ripple cross-laminated sandstone interval (F4A; Fig. 6A), interpreted to reflect sedimentation from a low-density turbidity current (Bouma T_C or T_{BC} units; Bouma 1962) that allowed grain-size sorting and the development of tractional bedforms (e.g., Lowe 1982). These deposits show reworked tops suggesting that peak flow turbulence took place after the deposition of the unit. Considering the overlying facies, this is

interpreted to indicate the initial increase of clay content during the early phase of the flow deceleration, and a change from turbulent flow (TF hereafter) to turbulence enhanced transitional flow (TETF hereafter; Baas et al. 2011). The peak-flow turbulence is interpreted to reflect lower transitional plug flow phase (LTPF hereafter; Baas et al. 2011).

- 2) The scoured top of the basal unit is sharply overlain by heterolithic, low-angle (ripple) cross-lamination (F3B; Fig. 6A). The heterolithic character of this unit is formed by alternating well-sorted sandstone and poorly sorted muddy sandstone lithosomes. Considering the



FIG. 6.—Examples of fine-grained density-flow deposits and small-scale hybrid beds. Facies, interpreted flow phases (after Baas et al. 2009; Baas et al. 2011), and hybrid-bed division (after Houghton et al. 2009) are shown. **A**) Four normally graded beds showing variable facies-motif development. The lowermost bed shows a scoured base overlain by mudstone-draped ripple-cross-laminated (F4B; TETF?, turbulent enhanced transitional flow?; LTPF, lower transitional plug flow) interval. Red arrows point to examples of putative countercurrent ripples. The foresets grade into incipient heterolithic interlamination (F3A) at the boundary to the overlying silty mudstone (F2A; UTPF, upper transitional plug flow). The uppermost bed contains a flat-based basal Bouma T_{bc} unit (F4A) that shows a scoured top (yellow arrow). This surface is sharply overlain by heterolithic, low-angle ripple cross-lamination (F3B). Blue arrow points to lamina termination to the overlying silty mudstone (F2A). The silty mudstone is sharply overlain by interlaminated silt and clay (T, minor turbulence, S, dilute suspension settling). The two beds in the middle of the photo lack a cross-laminated base, but show a basal sandstone streak, overlain by silty mudstone where most sand-size grains are enriched in the lower part of the bed. Hp, hemipelagic sedimentation. **B**) Close up to previous photo illustrating F4B–F3A–F2 gradation. **C**) An example of basal sandstone streaked unit (F4C) overlain by sandy–silty mudstone (F2) (see Fig. 6D for details) that forms flame structures (yellow arrow) in the overlying fine-grained structureless sandstone (F4D; H1 of Houghton et al. 2009). H1 is overlain by variably developed banded unit (F5B; H2) overlain by thin interval of muddy fine-grained sandstone (F6A; H3; QLPE, quasi laminar plug flow), which is further overlain by ripple cross-lamination. Green arrows indicate the appearance of incipient banding. Blue arrows point to small-scale loading structures. **D**) Close-up of bed showing basal sandstone streaked unit (F4C) overlain by sandy–silty mudstone (F2). Sand is enriched in the base but is sporadically present also in the upper part of the bed. The basal heterolithic unit contains laterally discontinuous lenses, which locally show diminutive ripple form (orange arrow). **E**) Sandy–silty mudstone bed (F2) that forms loading structures into the underlying mudstone bed. The bed is overlain by structureless sandstone that shows enrichment of organic matter and mud clasts towards the top of the unit. A thin and irregular interval of sandy mudstone (H3) overlies the unit. Blue arrow, water-escape structure, yellow arrow, flame structure.

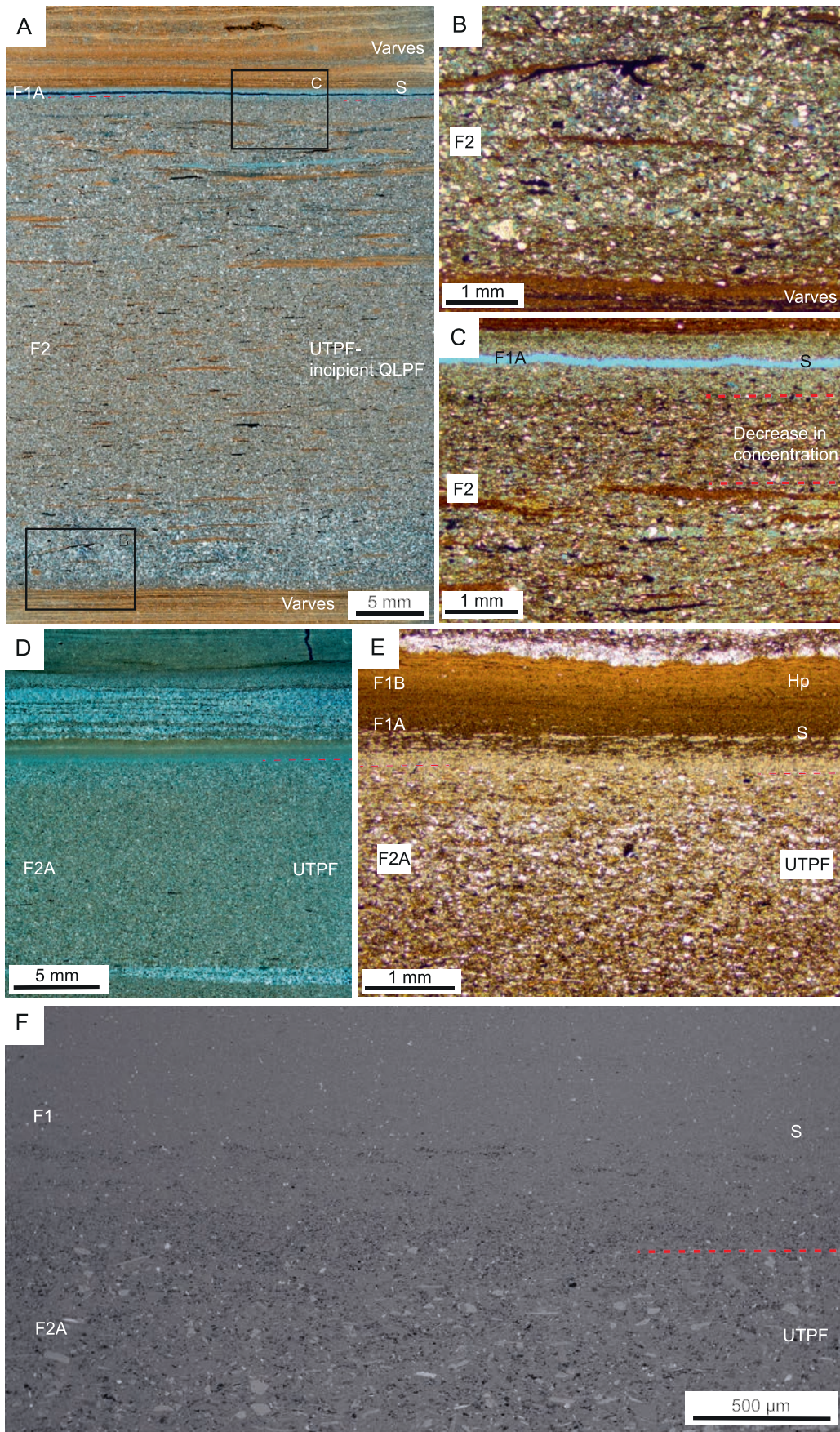


FIG. 7.—A–E) Micrograph examples of fine-grained density-flow deposits that lack or show limited basal well-sorted sandstone facies. **A)** Silty mudstone bed with sporadic sand-size grains (F2) that overlies varve sediments with a sharp unerosional contact. Note the concentration of sand-size grains in the lower part of the bed. Elongated mud clasts and local sand-size grains are also enriched in the upper part of the bed. **B)** A detailed view of the lower contact illustrating a laterally variable, inversely graded base up to 1 mm thick. **C)** A detail view to the upper part of the bed. The figure shows a mud-clast-rich silty mudstone that is sharply overlain by a well-sorted mudstone drape (F1A; S, dilute suspension settling). **D)** A millimeter-scale sandstone lens overlain by a silty mudstone unit. **E)** A detailed view of the upper part of the bed, showing inversely graded top, sharply overlain by a claystone drape (S), which grades upward into sideritic microlaminated clay (F1B; Hp, hemipelagic settling). **F)** Backscatter scanning-electron-microscope image of the boundary between silty mudstone and claystone drape (S).

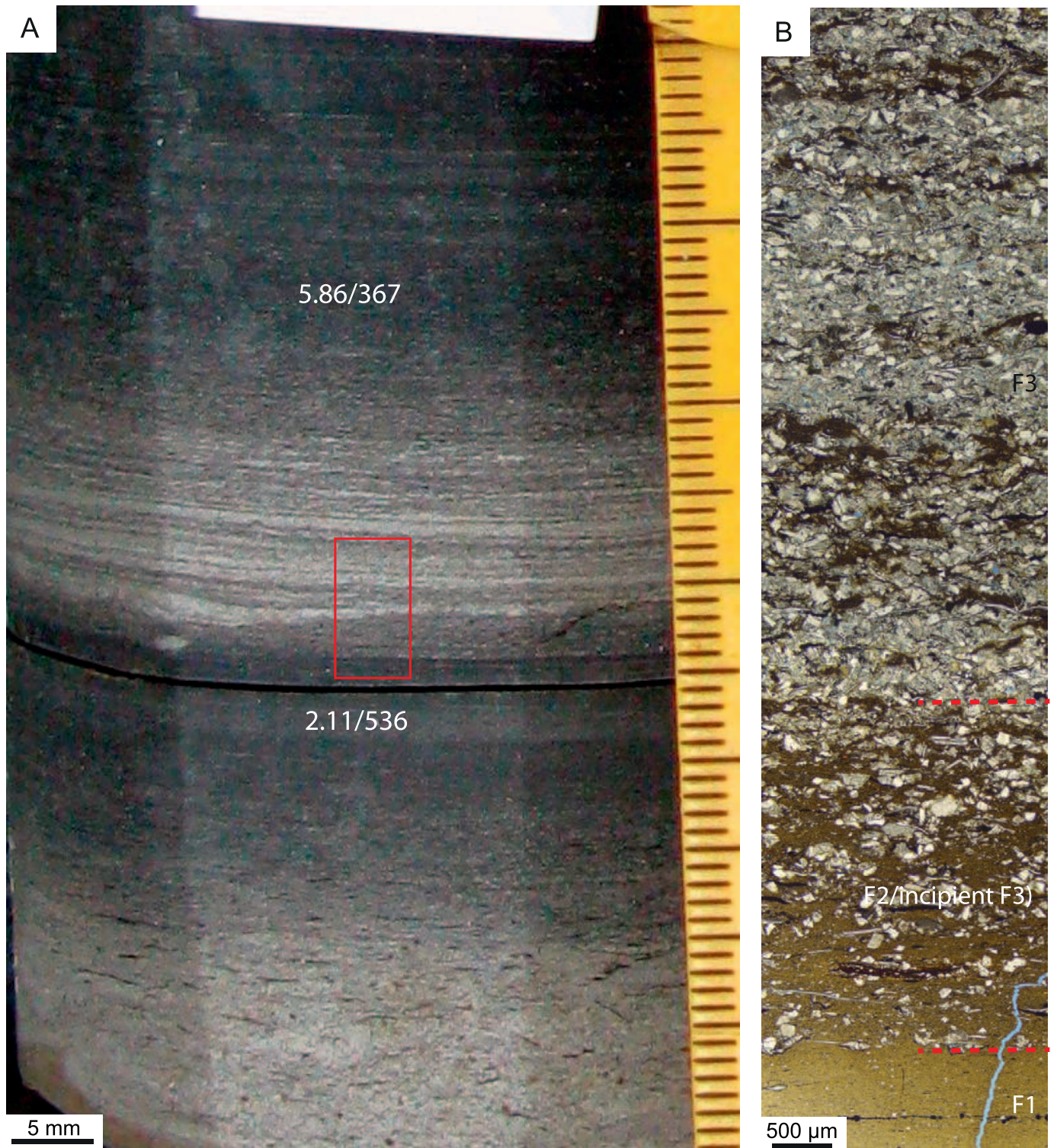


FIG. 8.—**A**) Macroscopic view of an inversely to normally graded bed comprising structureless mudstone and heterolithic interlamination. Source-rock screening data (TOC/HI) are shown. **B**) Thin-section micrograph illustrating the inversely graded interval (approximate location indicated by a red box in Part A). The deposits consist of mudstone (F1), sandy mudstone (F2B, incipient F3), and laminated sandy siltstone with diffuse mudstone-dominated interlaminae (F3).

presence of mud-rich poorly sorted lithosomes, the low foreset angle and the position of the facies below transitional plug flow (F2A; see below), the unit is interpreted to record suppressed turbulence and the final phase of ripple development during the late LTPF.

3) This unit comprises ungraded silty mudstone with very sporadic fine-sand grains (F2A). Silt-size grains are typically dispersed throughout the facies, but sand grains (if present) and coal fragments are more commonly enriched in the lower part. This suggests that the cohesion

TABLE 2.—The main facies and sub-facies used in this study. Flow phases are after Baas et al. (2009, 2011): TETF, turbulence-enhanced transitional flow; LTPF, lower transitional plug flow; UTPF, upper transitional plug flow; QLPF, quasi laminar plug flow. K-H, Kelvin-Helmholtz instability.

Facies	Occurrence	Sedimentology	Interpreted Process/Deposit Type
Mudstone-Dominated Density-Flow Deposits			
F1: Mudstone			
F1A: Laminated mudstone (Figs. 6, 7)	Sharply overlies F2, gradationally underlies F1B. Also present in sand-dominated density flows above F6.	Laminated mudstone comprising sub-mm-thick, well-sorted mudstone laminae. Locally (in ripple-cross-lamination-based beds) present are sub-mm scale, well-sorted siltstone streaks or discontinuous lenses at the boundary to the underlying silty mudstone. The unit is normally ~ 1 mm thick, but may reach a thickness of a few mm.	Dilute suspension settling, locally influenced by minor turbulence (silt streaks). Siltstone laminae and lenses are present only in beds that contain cross-laminated base, but are lacking from other bed motifs. This suggests that only the first mentioned had enough velocity for development of minimal turbulence at the top of the bed.
F1B: Sideritic microlaminated mudstone (Fig. 7)	Gradationally above F1A, forms background sedimentation between event beds in the upper part of the core	Micro-laminated claystone and sideritic claystone. The unit is ~ 0.5 mm to a few cm thick and may grade further upwards into regular, laterally continuous, micron-scale interlamination of microporous mudstone and silty mudstone (Fig. 7A). The porous interlaminations are often rich in diagenetic microcrystalline quartz. The lamina-couplet thicknesses range from 100 to 500 µm. The number of lamina couplets in between event beds is variable, ranging from 0 to at least several tens of couplets.	Hemipelagic sedimentation, locally develops varves. The microporosity in varves is tentatively interpreted to be due to dissolved diatoms.
F2: Silty mudstone (Figs. 6, 7)			
	Overlies F3 relatively sharply or forms the base of the bed set. Underlies F1A. Also present in sand-dominated density flows: F2A overlies F5A and occurs as discrete lithosomes in F5B.	Tabular, mainly ungraded beds ~ 1 cm to a few cm thick. Contains dispersed outsized silt (F2A) and rare sand grains up to 200 µm (F2B). Sand-size fraction, when present, is mostly enriched in lower part of the unit, but occur sporadically throughout the unit. Locally present are organic debris and lenticular small-scale mud clasts, which can be enriched in the lower and top parts of the bed (Fig. 7A–C). F2 forms flame structures into the overlying sandstone bed, show loading structures, or can be slump-folded when F1 is not developed.	F2A is interpreted to represent UTPF. Examples showing rare dispersed sand grains (F2B) approach low concentration QLPF (<i>sensu</i> Baas et al. 2011). Low-velocity flows.
F3: Heterolithic lamination or cross-lamination			
F3A: Heterolithic parallel lamination (Fig. 8)	Gradationally overlies F4B or F2. Underlies F2.	Heterolithic parallel lamination shows clean coarse siltstone–very fine grained sandstone laminae, which alternates with mudstone-rich laminae. The lamina set is variably developed and can be ~ 1–~ 10 mm thick when overlying F4B. Alternatively, F3A can gradationally overlie silty mudstone and grade upward back into the same facies, forming an inversely to normally graded lamina set. Such occurrences are up to a few cm thick (Fig. 8).	Sedimentation in the shear layer below UTPF. Minor K-H or comparable instability under slow-moving plug flow?

TABLE 2.—Continued.

Facies	Occurrence	Sedimentology	Interpreted Process/Deposit Type
F3B: Heterolithic low-angle cross-lamination (Fig. 6A)	Rare facies, overlies sharply F4A, underlies F2.	Low-angle heterolithic cross-lamination consists of sandy mudstone and well-sorted sandstone laminae. Lamina set is normally ~ 5 mm thick. The laminae sharply overlie the scoured top of F4A unit, and shows levelling out lamina terminations in the top. The foresets comprise lamina couplets that show basal silty-sandy mudstone, which grades upward into clean sandstone or siltstone lamina.	Suppressed turbulence below TPF during the late LTPF. Minor K-H or comparable instability under slow-moving low-concentration plug flow?
F4: Sandstone			
F4A: Parallel-laminated and/or ripple cross-laminated sandstone (Fig. 6A)	Base of a bed. Overlain by F3. Also present in sand-dominated density flows.	Flat-based, a few-cm-thick very fine- to fine-grained sandstone showing parallel-laminated and/or ripple cross-laminated intervals. The top or upper part of the unit shows scours and reworking.	Low-density turbidity current, T_{BC} or $T_{C,Bouma}$ (1962). Peak flow turbulence in top or upper part of the bed.
F4B: Heterolithic ripple cross-lamination (Figs. 6A, B)	Base of a bed. Overlain by F3A.	Scour-based, ripple cross-lamination with muddy toe-sets. The unit is 1–2 cm thick. The basal surface is directly overlain by a thin, mm-scale interval of clean sandstone that can be structureless and/or show small-scale, possible diminutive backflow ripples. The foreset angle of the main ripple unit decreases upward as they grade into F3A at the top.	Modulated turbulence (TETF?-LTPF). Foresets with variable angle, and superimposed putative back-flow ripples point to enhanced ripple lee-side turbulence. Basal scour suggests that peak flow turbulence coincides with the base of the bed.
F4C: Sandstone lenses and streaks (Fig. 6D)	Base of a bed. Overlain by F2.	Flat-based, sub-mm- to mm-scale, siltstone to very fine sandstone streaks or lenses that locally form micro-scale ripples overlain by sub-mm-scale mudstone drapes.	Minor residual turbulence under near-bed UTPF.
Sandstone-Dominated Density-Flow Deposits			
F4D: Structureless sandstone (Figs. 6 C, E, 11)	Base of a bed. Overlain by F5 or F6A.	Sharp-based, dm- to m-scale, fine- to medium-grained sandstone. The base may show flame structures rising from the mudstone below. The top of the unit is sharp or gradational, and the facies is overlain by banded unit (F5B; H2 of Haughton et al. 2009) or mud-clast-poor muddy sandstone (F6A; H3 of Haughton et al. 2009). Mud clasts and terrestrial organic matter are typically enriched near the top of the unit. Water-escape structures are locally present. Moreover, the deposits may show sharp internal surfaces across which color (pale to gray), organic-matter content and/or grain-size and sorting changes (Fig. 11A). Mineralogically F4D represents arkose sandstone, and is typically moderately to poorly sorted with angular to subrounded grains (Phuong 2014). Various rock fragments are present in smaller amounts.	High-density turbidity current, T_A (Bouma 1962), H1 (Haughton et al. 2009).

TABLE 2.—Continued.

Facies	Occurrence	Sedimentology	Interpreted Process/Deposit Type
F4E: Deformed gray sandstone (Fig. 12)	Base of a bed. Overlain by F6B.	Sharp-based, ~ 10 cm to ~ 1 m-thick, medium-grained, poorly sorted gray sandstone with minor detrital clay. The amount of detrital matrix is difficult to estimate due to authigenic clay. The sand-size fraction ranges from very fine to very coarse. F4E is fully deformed by water-escape processes.	Mixing of water and debris flow at the head of the flow?
F5: Banded unit			
F5A: Heterolithic interlamination to cross-laminated sandstone (Fig. 13A)	Base of a bed. Shows commonly deformed contact to underlying silty mudstone. Overlain by up to m-thick occurrences of F1A/F2A.	Cm- to a m-thick unit showing interbedded layers of fine-grained ripple cross-laminated and/or parallel-laminated sandstone and interlaminated mudstone and sandstone. The most sand-dominated occurrences show irregular mud flasers and lack continuous mud lamina, whereas mud-dominated examples lack cross-laminated layers. F5A is composed of arkose sandstone with variable sorting (good to poor) and grain shapes (angular to rounded) (Phuong, 2014). Common small-scale soft-sediment deformation and water-escape structures.	Transitional flow characterized by fluctuating turbulence. Develops under TETF-TPF. Lower sediment concentration than in F5B. K-H or comparable cyclic instability.
F5B: Banded structureless sandstone to silty mudstone–sandy mudstone (Figs. 11A, 13B)	Overlies F4D, overlain by F6A. Forms locally complex interbedding with F6A in beds that lack F4D.	Cm- to dm-scale unit comprising interbedded gray sandy mudstone, muddy fine-grained sandstone, and pale structureless sandstone. Lithosome composition is variable. The base of the gray muddy sandstone–sandy mudstone is often sharp near H1, whereas the pale sandstone may gradationally overlie it, forming inverse grading (Fig. 11A). However, towards H3 the pale sandstone shows more commonly sharp and loaded base. In these cases, the pale structureless sandstone shows normal grading and may contain flame structures rising from the silty or sandy mudstone laminae below. Water-escape structures occur commonly at H1–H2 boundary, and they may truncate against the sharp-based, gray muddy sandstone lithosome (Fig. 11A). In a single case, the sandy mudstone showed an internal, a few-mm-thick interval of heterolithic interlamination similar to F3A (Fig. 13B).	Transitional flow characterized by fluctuating grain support capacity. Develops mainly under TPF-low concentration QLPF. Higher sediment concentration than in F5A. K-H or comparable cyclic instability. H2 of Haughton et al. (2009).
F6: Muddy sandstone (Figs. 11, 12, 13B)	Overlies F5, F4, or forms the base of the bed set. Overlain by F4A, F2A, and F1.	F6 ranges from cm-scale muddy sandstone (F6A) to dm- and m-scale extraformational clast and cm-scale mud-clast-bearing muddy sandstone or sandy mudstone (F6B). The outsized extraformational clasts that are at least up to granule size, angular, and contain of various rock fragments.	QLPF, H3 of Haughton et al. (2009), F6A low strength cohesive debrite (D_{m-1}), F6B intermediate-strength cohesive debrite (D_{m-2}) (Talling et al. 2012b).

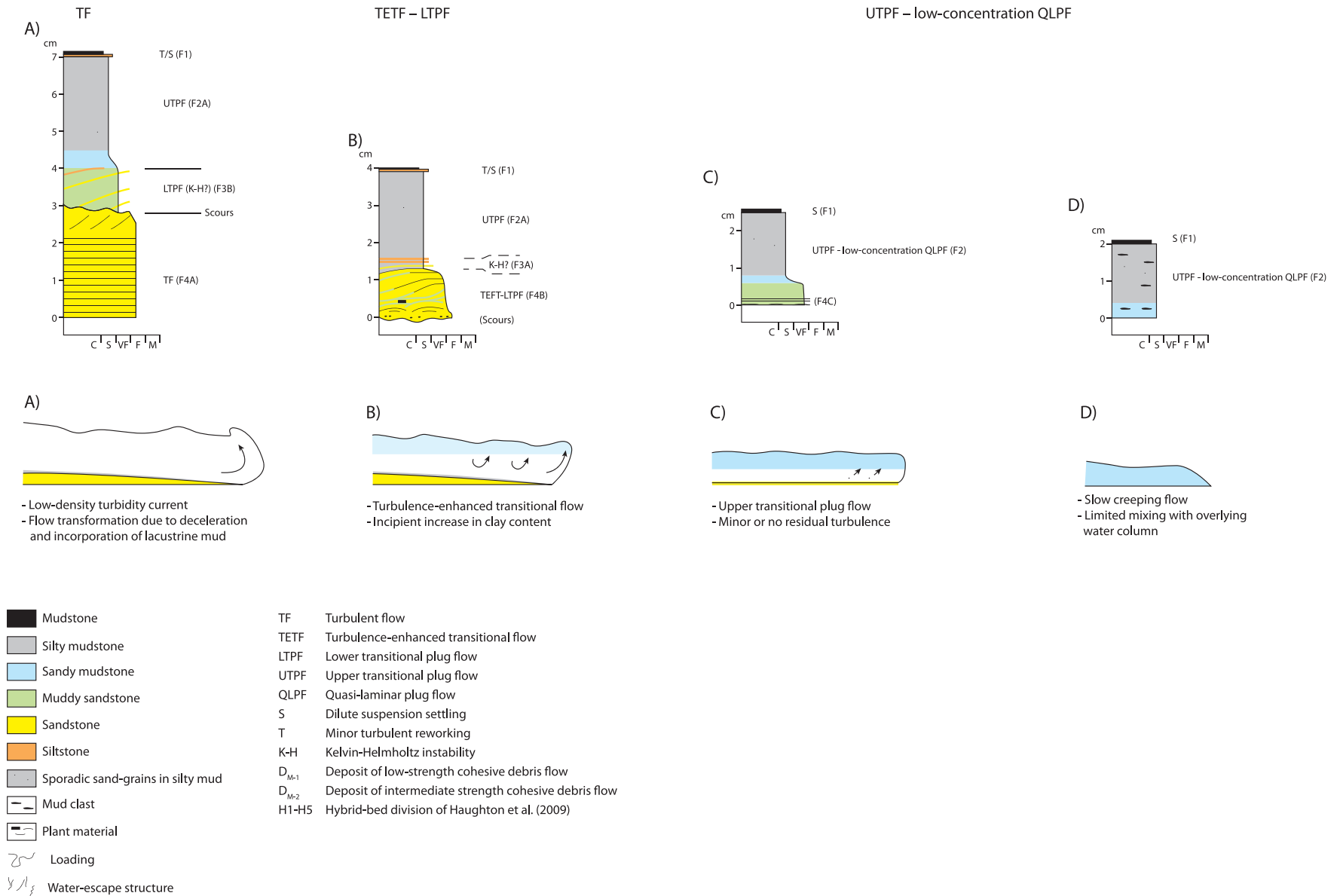


FIG. 9.—Schematic model illustrating the main bed-motif variability of fine-grained density-flow deposits. Typical thickness of the beds and inferred flow type are shown. The simplified sketches of flow structure aim to illustrate flow behavior at the start of deposition at the point of observation. Flow-phase vocabulary is mainly after Baas et al. (2009); debrite classification (used in Fig. 14) is after Talling et al. (2012b).

of the mud was commonly not sufficient to support most sand-size grains. Considering these properties and the ungraded top, the unit is interpreted to represent upper transitional plug flow (UTPF hereafter; Baas et al. 2009; Baas et al. 2011) deposits and thereby fluid mud (e.g., McCave and Jones 1988; Ichaso and Dalrymple 2009; Baas et al. 2011; Mackay and Dalrymple 2011). Common occurrences of soft-sediment deformation structures support this interpretation.

- 4) Finally, the plug-flow deposits can be abruptly overlain by well-sorted laminated mudstone (F1A) forming an intra-mudstone grain size break (Figs. 7C–F examples from other motifs). The unit is normally ~ 1 mm thick, but may reach a thickness of a few millimeters. Moreover, locally present are sub-millimeter scale, well-sorted siltstone streaks or discontinuous lenses at the boundary with the underlying silty mudstone. The facies change from poorly sorted and mainly ungraded plug-flow deposits to well-sorted, laminated mudstone with local silt streaks points to an abrupt decrease in sediment concentration and deposition via dilute suspension fallout and short-lived, very weak turbulent reworking that was able to sort silt- and clay-size grain-size calibers. The thickness (~ 1 mm after compaction) of the unit suggests negligible shear mixing between the plug flow and overlying water column, which is likely due to very low flow velocity. Moreover, the observations further suggest that the plug-flow mud layer and the overlying water column were probably separated by a sharp lutocline (interval of abrupt change in sediment concentration; e.g., McAnally et al. 2007) and the overlying water column was probably nearly clear of sediment as the majority of the event-related sediments were emplaced by the underlying density-flow processes. Finally, the dilute-suspension settling drape grades upward into hemipelagic microlaminated sideritic mudstone (F1B; Figs. 7D, E) and is locally further succeeded by well-defined varve facies.

Motif 2: Beds with Transitional-Flow-Ripple Bases (Fig. 9B).—Motif 2 is similar to motif 1, but the basal unit is interpreted to reflect modulated turbulence.

- 1) A basal, scour-based unit showing ripple cross-lamination with muddy toesets (F4B; Fig. 6 A, B). The ripple foresets show variable angle and probable back-flow ripples at the toesets (Fig. 6B), which point to enhanced ripple lee-side turbulence. The foreset angle decreases upward, suggesting the onset of decreasing turbulence and increasing near-bed sediment concentration. Thus, the unit is interpreted to reflect decelerating flows, where deposition started with the peak turbulence (TETF or LTPF) at the point of observation. The peak flow turbulence was followed by a declining turbulence phase after which ripples no longer develop; this is interpreted to reflect deposition during the LTPF regime (Baas et al. 2011).
- 2) The basal unit can be gradationally overlain by heterolithic parallel lamination (Fig. 6B incipient example; see also Fig. 8 for example from other motif). The heterolithic fabric is ideally formed by coarse silt to very fine-grained sandstone laminae, which alternates with mudstone-rich laminae. Locally the lamination is weakly developed. The facies shows an upward-increasing mudstone content and is normally a few millimeters thick. As mentioned above, the unit is positioned above an interval showing evidence of modulated turbulence, and is situated directly below a silty mudstone unit (F2A; fluid-mud plug). This suggests sedimentation in the shear layer that develops between the bed and the overriding transitional plug flow.
- 3) and 4) The two uppermost intervals are the same as in bed motif 1 described above.

Motifs 3 and 4: Plug-Flow-Based Beds (Fig. 9C, D).—Motifs 3 and 4 lack the cross-laminated basal unit and are typically thinner and more distal or lateral, being more commonly interbedded with the background lacustrine facies. The motif either starts directly from silty or sandy mudstone (F2; Fig. 7) or contains flat-based, sub-millimeter to millimeter-scale, very fine- to fine-grained sandstone streaks or lenses (F4C) that locally form micro-scale ripple forms (Fig. 6D). Considering that the unit occurs below the silty or sandy mudstone unit and the presence of micro-scale ripple forms, the unit is interpreted to reflect a narrow zone of residual turbulence below the approaching transitional or nearly laminar plug flow. In comparison to beds with a basal low-density turbidite (Motif 1), the silty–sandy mudstone unit shows increasing silt content and occurrence of sand-size grains (still sporadic, up to 200 μ m) and small-scale lenticular mud clasts, suggesting increasing cohesion and gradation towards the incipient quasi-laminar plug flow (QLPF hereafter). The smallest observed beds (~ 1 –2 cm) lack sand-size grains but are increasingly silt-rich (Fig. 7A). As with the bed motifs 1 and 2, a laminated mudstone unit forms the top of the bed, but lacks siltstone laminae.

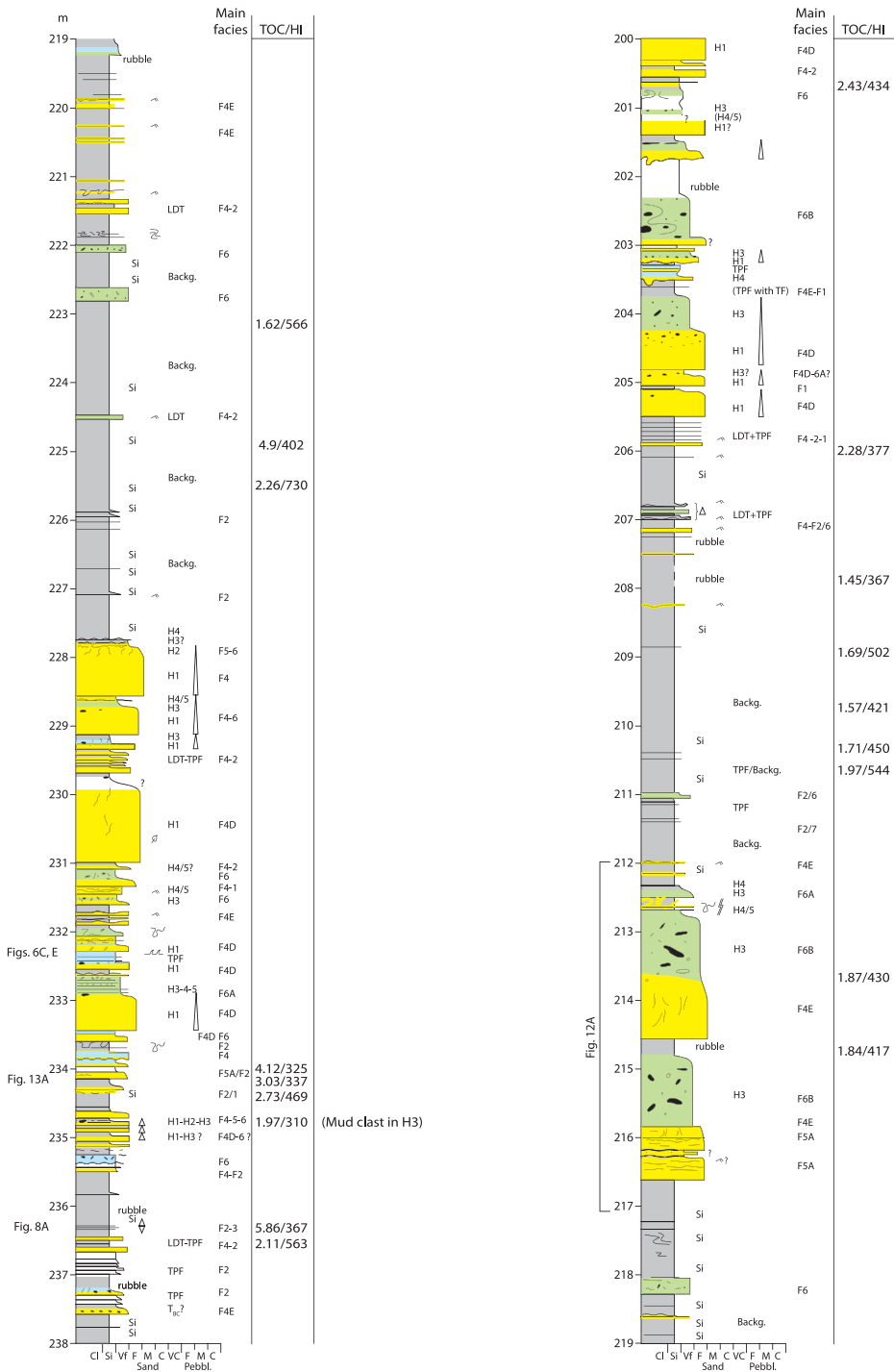
Finally, beds starting with silty mudstone can grade upwards to heterolithic parallel lamination (F3A), which grades back to silty mudstone, forming inversely to normally graded beds a few centimeters-thick (Fig. 8).

Sandstone-Dominated Density-Flow Deposits

Sandstone-rich density-flow deposits including hybrid beds are a common deposit type in the Enreca-3 core, and occur as solitary beds interbedded with background lacustrine sediments, or form meter-scale mainly upward-coarsening successions together with fine-grained gravity-flow deposits (Figs. 10–13). As in the fine-grained density flows discussed above, the bed motif varies according to flow conditions that prevail at the start of deposition at the observed point. Moreover, the resulting bed motif is closely related to the strength of the associated cohesive-debris-flow unit (Talling 2013). Facies and sub-facies are described and interpreted in Table 2, and the four main bed-motifs and their inferred flow evolution are summarized below.

Motif 5: Hybrid Beds (Fig. 14A, B).—Motif 5 comprises hybrid beds and shows two main variants: Variant A lacks a banded transitional flow unit, whereas Variant B contains the unit. Other differences relate to thickness and nature of the basal structureless sandstone unit.

- 1) The basal unit consists of fine- to medium-grained structureless sandstone (H1 of Haughton et al. 2009; F4A; Figs. 6, 11), a few centimeters to a meter thick, interpreted to represent a high-density-turbidity-current deposit (T_A of Bouma 1962; e.g., Lowe 1982; Haughton et al. 2009; Talling 2012b). The locally occurring abrupt changes in sorting and organic-matter content suggest changes in flow concentration during its deposition. Mud clasts are common and occur in particular near the top of the bed, and water-escape structures are variably present.
- 2) A banded unit (H2 of Haughton et al. 2009; F5B; Fig. 11A) is commonly present above centimeter- to decimeter-scale occurrences of H1, when the top of the H1 unit is relatively clean (visual inspection), lacks centimeter-scale mud clasts (cf. Haughton et al. 2009) and intense water-escape processes. It is normally lacking in beds that contain a thick (~ 1 m) H1 unit. The H2 unit is typically ~ 1 to ~ 10 cm thick and shows interbedded silty mudstone, sandy mudstone, muddy fine-grained sandstone, and pale structureless sandstone. The boundary between H1 and H2 is usually sharp (Fig. 11A), but locally the banding gradually becomes more pronounced upward (Fig. 6C). The individual lithosomes comprise mainly similar



- Mudstone
- Sandy mudstone
- Muddy sandstone
- Sandstone
- Siltstone
- Si Siderite
- Extraformational clast
- Mud clast
- Plant material
- Loading
- Water escape structure
- Slump fold
- Flame structures
- Plant fragments
- Intrusive sandstone
- LDT Low density turbidite
- TPF Transitional plug flow deposit
- H1-H5 Hybrid bed division (Haughton et al. 2009)

FIG. 10.—A sedimentological log illustrating distribution of hybrid beds and their characteristic facies successions. Source-rock screening data are shown.

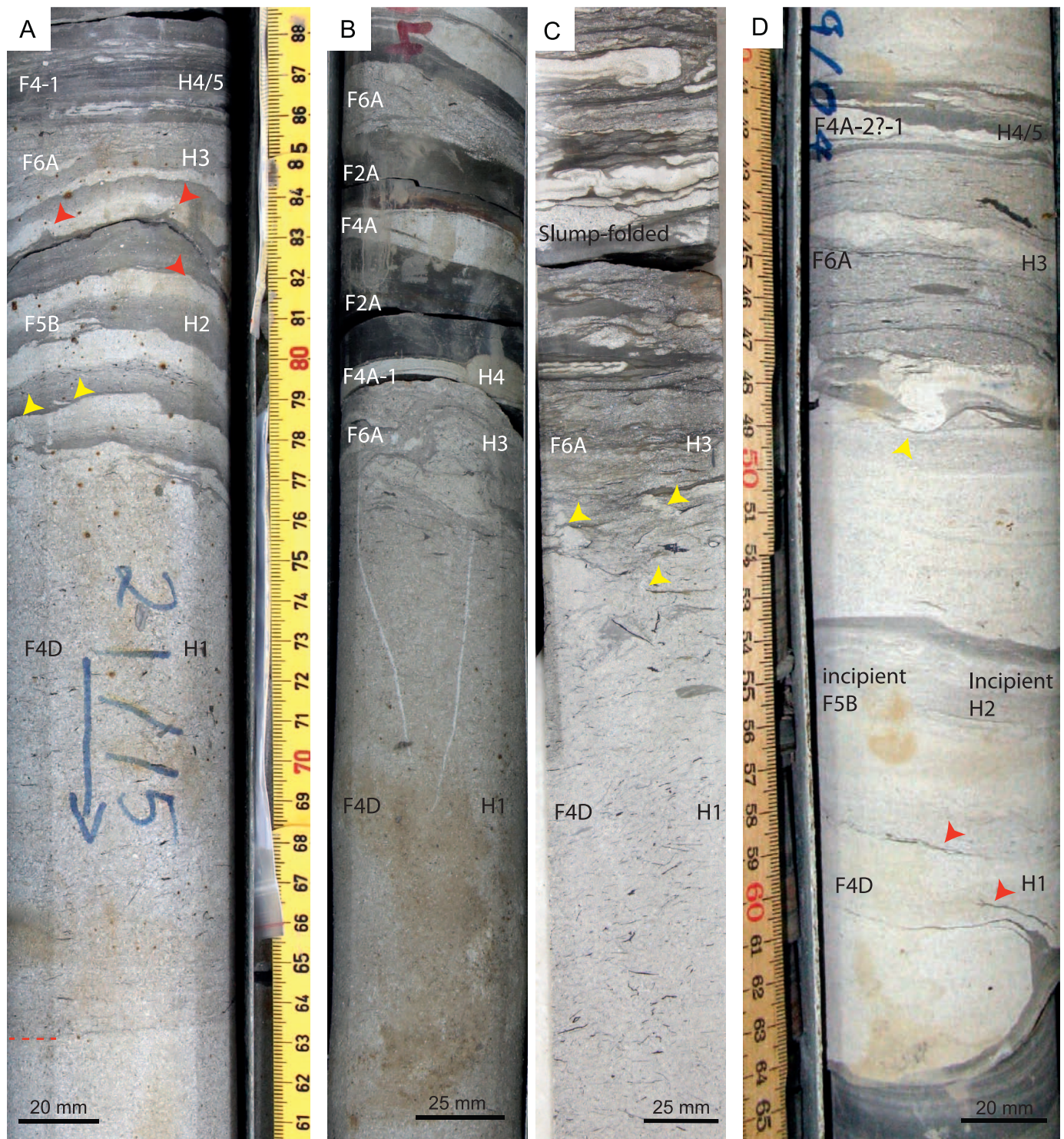
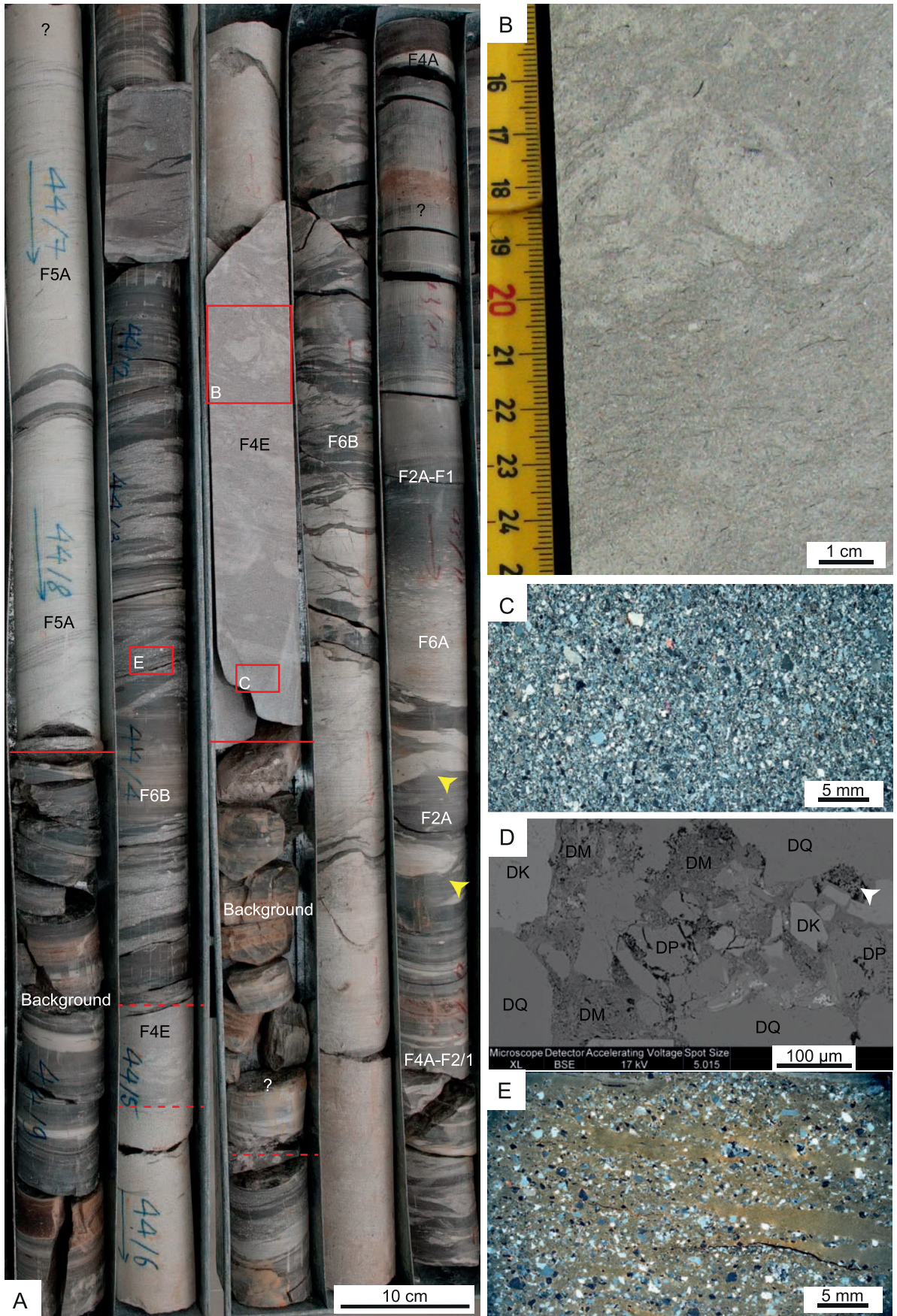


FIG. 11.—Examples of hybrid beds. **A**) Top part of an approximately 25-cm-thick structureless sandstone (F4D; H1) overlain by an interval of banded sandstone–muddy sandstone (F5B; H2), and further thin tabular unit comprising muddy sandstone (F6A; H3; D_{M-1} of Talling et al. 2012b). In the top, H3 is sharply overlain by millimeter-scale heterolithic interlamination showing local pseudonodular siltstone lenses (H4–5). Yellow arrows, water escape structures; red arrows, flame structures and mudstone injections; dashed red line, intra H1 boundary recording abrupt increase in organic-matter fragments. **B**) Top part of an approximately 22-cm-thick structureless sandstone (H1) overlain by chaotic muddy sandstone (H3), and ripple cross-laminated fine-grained sandstone topped by millimeter-scale clay drape (H4–H5). Top of the figure shows interbedded structureless clayey mudstone beds (fluid mud), ripple cross-laminated sandstone, and muddy sandstone (debrite) beds. **C**) Top of an approximately 25-cm-thick structureless sandstone (H1) overlain by a chaotic muddy sandstone interval (H3). The muddy sandstone is slump folded and mixed with well-sorted sandstone facies. **D**) Small-scale example of a hybrid bed. Flame structures are horizontally oriented (sheared?) and may follow the base of incipient banding (red arrow).



transitional units as described from individual muddy density flows above. Locally present are lamina-scale occurrences of QLPF facies (F6A; muddy sandstone). All the lithosomes present lack tractional bedforms, suggesting permanently higher sediment concentrations than in F5A (see Motif 8 below). The pale structureless sandstone with a loaded base forms gradational couplets with the transitional-plug-flow facies, which is interpreted to lack sufficient bed cohesion (and turbulence) to support sand-size particles. Thus, the structureless sandstone intervals may reflect vertical grain-size segregation from the near-bed low-strength plug flow (see Sumner et al. 2009; Baas et al. 2011). The stacking of these deposits points to repeated changes in flow concentration and alternations between suppressed turbulence and nearly laminar flow processes (see discussion).

- 3) An interval of muddy sandstone (H3 of Haughton et al. 2009) either overlies the H2 unit (Fig. 11A) or lies directly on H1 (Figs. 11BC). The unit is normally a few centimeters thick and lacks centimeter-scale clasts and shows grain size similar to or coarser than (sand fraction) the underlying facies (F6A). When H3 directly overlies H1, it normally shows a deformed lower contact, which is demarcated by an increasing matrix clay content. Water-escape structures are observed locally, in particular in the lower part of the bed. Coal fragments are common and can be enriched in the top of the unit. When the unit overlies H2, the contact is mostly sharp, although the individual mudstone-dominated components of H2 may show increasing sand content towards the H3 boundary.

The ungraded nature of the H3 unit and the poor sorting comprising mud- and sand-size grains indicate a debris-flow origin. The lack of centimeter-scale mud clasts, the thinness of the unit (a few centimeters thick), and the association with an up to meter-thick high-density-turbidite unit point to effective mixing. These observations are indicative of a low-strength cohesive-debris-flow origin (D_{m-1} ; Talling et al. 2012ab; Talling 2013).

- 4) The H3 unit is overlain by ripple cross-laminated sandstone (H4 of Haughton et al. 2009; F4A) and structureless few-centimeters-thick mudstone beds and/or laminated mudstone (H5 of Haughton et al. 2009; F2A and F1A; Figs. 11A–D). The laminated mudstone contains color-graded mudstone laminae and lacks signs of penecontemporaneous deformation. The interval may comprise a normally graded centimeter- to decimeter-scale bed, or show complex interbedding of the constituent facies, where differentiation between single flow units and stacked small-scale events is challenging. Locally the H4–H5 unit is slump-folded with H3 (Fig. 11C).

Gravity-flow-related ripple cross-lamination points to a low-density-turbidity-current origin for the H4 unit (T_C of Bouma 1962; Lowe 1982). The H5 unit is locally complex, containing both ungraded density-flow mudstone beds as well as graded suspension-fallout laminae. The locally occurring thick H5 intervals may point to effective shear mixing or reversing buoyancy in the top of the underlying debris flow.

Motifs 6 and 7: Intermediate-Strength Cohesive-Debrite-Bearing Beds (Fig. 14C, D).—The beds containing intermediate-strength cohesive

debrite (see below) produce at least two motifs: deformed sandstone-based beds and intermediate-strength cohesive-debrite-based beds.

- 1) The deformed sandstone-based beds show a basal decimeter- to a meter-thick gray sandstone unit, which is characteristically fully deformed by water-escape processes (F4E; Figs. 12A, B). The unit is moderately to poorly sorted, medium-grained sandstone with a subordinate detrital mud matrix (Figs. 12B–D). The delineation of the amount of detrital matrix is challenging due to presence of authigenic mud, but it is tentatively estimated to be less than approximately 5%. Considering the intense deformation due to water escape and its position directly under the mud-clast-rich cohesive debrite (F6B; see below), it is interpreted to represent “shear wetting” of the basal part of the debrite due to mixing of water and the debris-flow body at the head of the flow (Ilstad et al. 2004; Talling 2013). Ilstad et al. (2004) demonstrated experimentally that the heads of weakly coherent debris flows tend to show mixing of water with the lower part of debris flow due to high shear, which leads to deposition of basal sand-rich watery sediments. Talling (2013) suggested that such a process may be common in submarine debris flows and would generate homogenized layers of sediment with a high water content and lower sediment concentrations than the overlying debrite, similar to the facies observed here.
- 2) The deformed sandstone unit is overlain by several decimeters- to a meter-thick muddy sandstone or sandy mudstone unit characterized by centimeter-scale mud-clasts and at least up to granule-size extraformational clasts (F6B; Figs. 12A, E). The thickness of the unit and centimeter-scale mud clasts suggests that the flow may have reached intermediate strength during the late stage of the flow (D_{m-2} ; Talling et al. 2012a; Talling et al. 2012b; Talling 2013).
- 3) The top of the bed is formed by a thin H4 and H5 unit, but an H2 unit was not observed.

Motif 8: Beds with Basal Low-Concentration-Transitional-Flow Deposits (Fig. 14E).—The basal unit of motif 8 is banded and shows low-density-turbidite-bearing intervals.

- 1) The basal unit is approximately 10 cm to 1 m thick, and is composed of bands of interlaminated mudstone and fine-grained sandstone laminae, which are interbedded with intervals of ripple cross-lamination and parallel lamination (T_C/T_B of Bouma 1962; Fig. 13A). The sandstone band can be loaded into the underlying mud-laminae-rich band. The ripple foreset angle is highly variable, ranging from steep to nearly flat, where foresets can be distinguished only by base-lapping lamina contacts. The upper contact of sandstone band to mudstone-laminae-rich band locally shows small water-escape structures (Fig. 13A). The sandstone-dominated end members show irregular, wispy, laterally discontinuous mudstone-laminae flasers, whereas mudstone-dominated examples lack cross-laminated bands and show only interlaminated mudstone and sandstone. F5A may show both normal and inverse grading. The variable foreset-laminae angle and sorting as well as the alternating

Fig. 12.—**A**) Examples of decimeter-scale occurrences of F6B bearing mud clasts and outsize extraformational clasts and the underlying deformed gray sandstones (F4E). Base of the core is on lower left. Note also the F5A occurrence. Yellow arrow, sandstone intrusion. **B**) Close-up of gray sandstone intensely deformed by water-escape processes (F4E). **C**) Thin-section micrograph (crossed nicols) of the previous facies. The deposits are moderately to poorly sorted, the mean grain size being medium sand. The sand size fraction ranges from very fine to very coarse, and the deposits contain a minor amount of mud matrix. **D**) Backscattered scanning electron microscope image of the previous thin section showing the distribution of detrital sand and silt grains and detrital matrix. Detrital sand and silt grains comprise quartz (DQ), K-feldspars (DK), and plagioclase (DP). The fine-grained matrix (DM) fills the intergranular pore spaces and consists mainly of detrital and authigenic clay (mostly kaolinite) as well as mica. Some authigenic kaolinite occurs as vermiciforms and booklets, and also authigenic microcrystalline quartz (white arrow) occur in open pore spaces. **E**) Thin-section micrograph (crossed nicols) of muddy sandstone–sandy mudstone (F6B) overlying a deformed gray sandstone. Extraformational clasts are up to granule size, the mean sand fraction being upper medium. The clasts are subangular to angular and contain rock fragments of various origins.

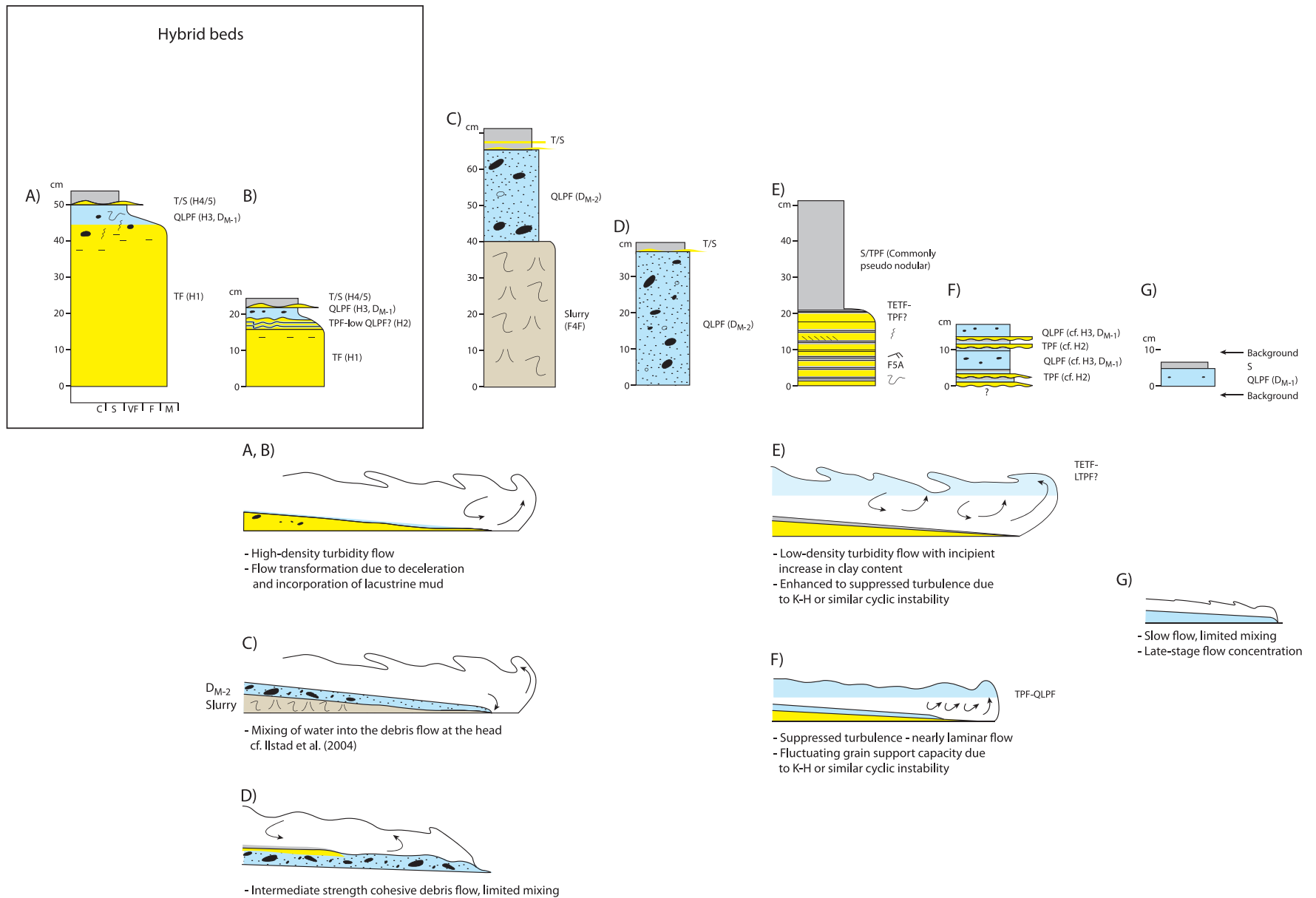


FIG. 14.—Schematic model illustrating the main bed-motif variability of hybrid beds and other decimeter- to meter-scale density-flow beds. Typical thickness of the beds, inferred flow type, and their deposits are shown. The simplified flow-structure sketches aim to illustrate flow behavior at the start of deposition at the point of observation. Sketches of flow structure are inspired by Haughton et al. (2009). See Figure 9 for legend.

interlaminated bands lacking ripples point to fluctuating turbulence with periods of suppressed turbulence.

- 2) The basal unit is overlain by a silty mudstone unit that can be several centimeters to a meter thick and is commonly pseudonodular. Locally present deformed siltstone laminae suggest that the unit represents initially low-concentration suspension. Considering this, the basal ripple cross-lamination-bearing banded unit is interpreted to have formed under incipient plug flow characterized by modulated turbulence, similarly to F4B (TEFT-LTPF; Baas et al. 2011; see Discussion).

Motif 9: Interbedded Transitional-Flow Deposits and Debrites (Fig. 14F).—Banded transitional flows with a higher sediment concentration (cf. H2) may form complex motifs with reverse and repeating trends with low-strength-debris-flow deposits (H2–H3–H2; Figs. 13B, 14F). The origin for this complexity is enigmatic; hypothetically it could be due to multiple slump events at various locations along the lake slope, or flow reflection due to the narrow fault-bounded basin morphology (see Discussion).

Motif 10: Low-Strength-Debrite-Based Bed (Fig. 14G).—Muddy sandstone (F6A) can form solitary beds a few centimeters thick that are interbedded with background mudstone. The muddy sandstone interval can be overlain by thin mudstone laminae (F1A).

Source-Rock Screening Results

Thirty samples representing four different facies, silty mudstone (F2A; Transitional Plug Flow, TPF; 18 samples), deformed mud clasts or mud intrusions in structureless sandstone (F4D; H1; 2 samples), mud clasts in muddy sandstone (F6; H3; 3 samples), silty mudstone and laminated mudstone from the top of hybrid bed (F2A, F1A; H5; 6 samples), and silty mudstone (F2A; H5 or individual TPF bed; 1 sample) were analyzed (Fig. 12). Organic-carbon contents range from 1% to nearly 7% by weight, and the carbonate content is highly variable, but the sulfur content is invariably low. The petroleum potential is high, with values of S₂ in the range 4–28 mg HC/g rock. Derived-hydrogen-index values are high, ranging from slightly less than 300 to more than 600 (Fig. 15), and all samples are thermally immature.

Interpretation of Screening Data

In the absence of differences in thermal maturity, the observed variation in source-rock screening results (Fig. 15) is attributed to variations in the chemical composition of the kerogen, probably caused mainly by differences in the degradative state of the kerogen, compounded by variation in a presumably minor input of terrestrial kerogen to the predominantly aquatic kerogen. Based on Rock-Eval data, the kerogen can be classified as predominantly oil-prone type II, but ranging in composition between transitional types I–II and II–III. Irrespective of facies assignment, all samples fall within the range in Hydrogen Index defined by the TPF facies, suggesting that all the kerogen present has roughly the same origin (e.g., Bordenave et al. 1993; Peters and Cassa 1994). None of the density-flow facies represented in the dataset form clearly defined populations that can be unambiguously distinguished from any other facies. Hence, the kerogen presumably mostly represents autochthonous lacustrine deposition of both epilimnetic (above the pycnocline, i.e., layer of water in which density increases rapidly with depth) and hypolimnetic (below the pycnocline) environment; the differences in the potential for organic-matter degradation in these two settings will lead to lower and higher values of the Hydrogen Index, respectively (Piasecki et al. 1990; Bohacs et al. 2000; Carrol and Bohacs 2001).

DISCUSSION

Previous studies have indicated that hybrid beds are a common feature of many distal basin-floor settings in marine environments. The results of this study show that they also occur in freshwater lacustrine basins and can be an important constituent of rift-lake systems. The hybrid bed motifs of the Enreca-3 core include beds (H1–H5) essentially similar to those described from marine basins (Haughton et al. 2009; Talling 2013). This suggests that water chemistry has only a secondary influence at most on flow transformation and concentration, and that it can be masked by other factors such as clay mineralogy (here mainly illite and kaolinite; Phuong 2014) and organic-matter content. This theme, in particular what type of organic-matter compounds can affect colloidal properties of clays in fresh water lakes, requires future work.

The observation of lacustrine hybrid beds contributes not only to the understanding of how and where hybrid beds can develop, but also to exploration models in rift-lake systems, which form a primary play type in Southeast Asia and East Africa, for instance. Cohesive debrites, such as those associated with hybrid beds, are in general characterized by low permeability and can thus form flow barriers in hydrocarbon reservoirs. Most of the debrite intervals in the studied hybrid beds are thin, assigned to late-stage flow concentration and thus can be expected to pinch out up-dip.

In addition to “classic” hybrid beds, the Enreca-3 core contains common mudstone-dominated centimeter-scale beds that deviate from the standard hybrid bed model, but show similar evidence of flow transformation during single flow events. The flow evolution of the most complete centimeter-scale beds is interpreted to reflect TF–TETF–LTPF–UTPF overlain by dilute suspension settling (S) and locally minor turbulent reworking (T) at the top (Fig. 9). This is broadly analogous to the ideal hybrid bed motif that comprises a turbulent flow unit (H1 = TF), a transitional flow unit (H2 = TEFT–UTPF), a laminar-flow unit (H3 = QLPF), and a turbulent and suspension-settling unit at the top (H4–5 = T-S) (Haughton et al. 2009; Baas et al. 2011; see below). The main difference is that the plug flow did not reach a true laminar state in the centimeter-scale beds. It is possible that such small-scale density-flow beds are better developed in freshwater than in marine settings due to the lower water density, which allows density-flow deposition at lower sediment concentrations. Moreover, the water density difference should have an effect on processes such as mixing and the tendency for reverse buoyancy. Hypothetically, this could lead to deposition of thicker suspension deposits on top of the plug-flow mud in the marine realm, for instance.

The main reasons why hybrid beds and transitional-flow facies in particular are so well developed in the studied rift lake probably relate to: 1) a soft, muddy lake floor and its proneness for flow-substrate interaction; and 2) the narrow syntectonic basin characterized by collapse-triggered sediment gravity flows. These themes are discussed further below.

Interaction between Flow and Lake Floor

Several recent studies have indicated that the flow behavior of turbidity currents is highly sensitive to sediment (and clear-water) entrainment (see Traer et al. 2012 and Traer et al. 2015 for mathematical considerations) and that flow-substrate interaction can be a significant process, particularly when gravity flows override muddy unconsolidated substrates. Baas et al. (2014) showed experimentally that cohesionless turbidity currents are able to enter fluid-rich muddy substrates and produce a complex set of facies including turbidites with internal mud layers, mixed cohesive–noncohesive sediment layers, and various soft-sediment-deformation structures. Moreover, the interaction may result in the development of various syndepositional shear structures (Butler et al. 2016), or the mud can be assimilated into the density-flow body and modulate its turbulence (Verhagen et al. 2013). Considering that even small increases in the clay content of the flow can damp turbulence and transform the flow towards a laminar state as

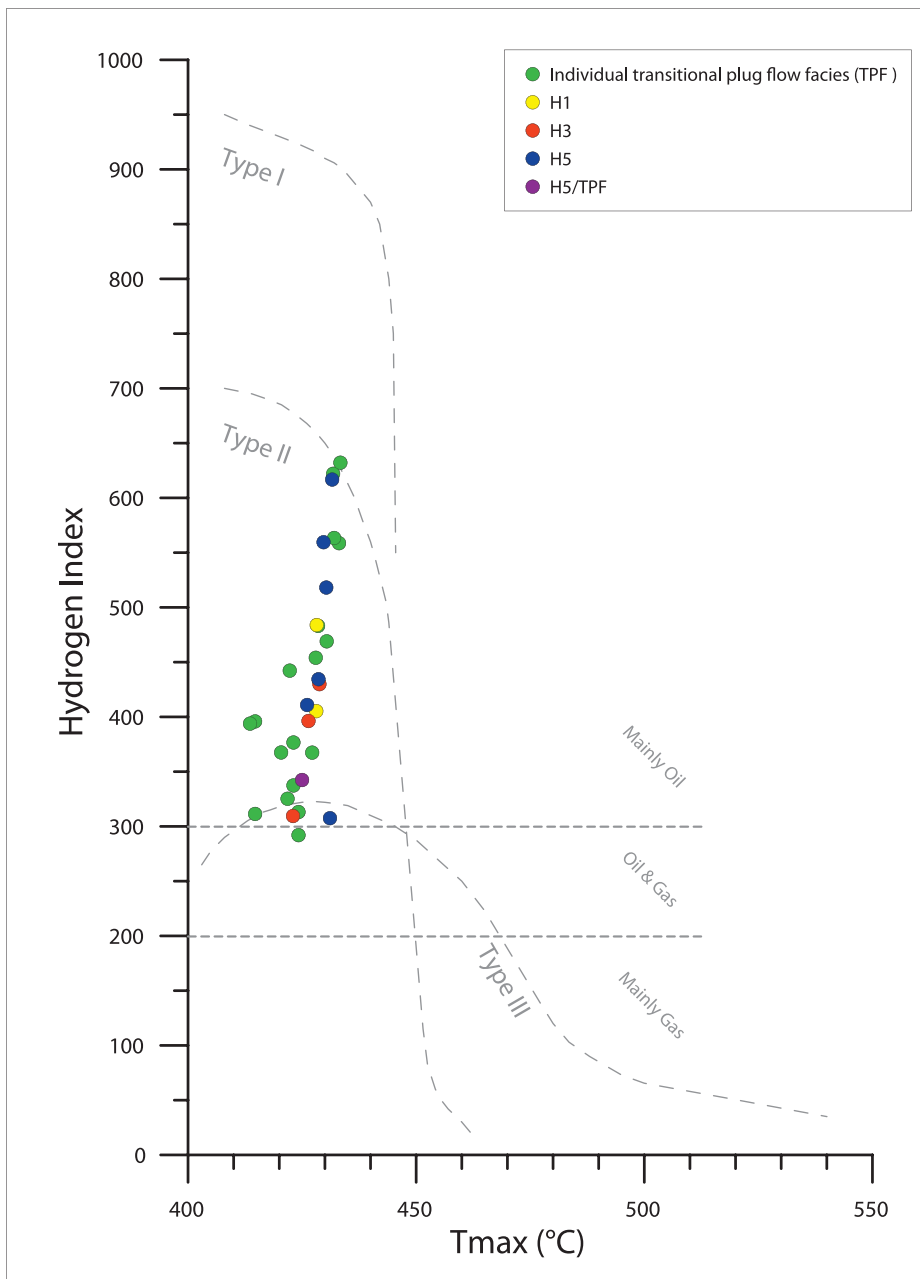


FIG. 15.—Hydrogen Index, T_{max} ($^{\circ}\text{C}$) graph illustrating kerogen type of the analyzed samples. H1–H5, hybrid divisions of Haughton et al. (2009). H3 samples are mainly deformed mud-clasts, whereas H1 samples are either deformed clasts or mud intrusions or interbeds. TPF, individual transitional plug flow deposits not associated with the classic hybrid beds. See text for discussion.

the flow decelerates (Baas et al. 2009; Baas et al. 2011; Sumner et al. 2009), even minor incorporation of the lake-bottom mud into the density flow can be expected to have a significant effect on flow dynamics.

The results of source-rock screening in this study indicate that the analyzed mudstone samples including mud clasts in the H3 unit represent mostly lake-floor and lake-margin mud, and were not directly supplied by rivers. These findings are surprising considering that macroscopic observations revealed the common presence of plant debris such as leaves especially in the basal structureless sandstone facies. This points to different sources for the sandstone and much of the mudstone in the hybrid beds. The sands were probably derived from shallow parts of the lake or subaerially exposed areas near the lake such as rift shoulders, whereas most of the mud must have been assimilated into the density flow in the lake basin. The latter interpretation is supported by sedimentological data that show common indications of interaction between the lake-floor sediments

and the overriding density flow such as asymmetric flame structures (cf. Butler et al. 2016), deformed mud intrusions and interbeds in turbidite facies, loading structures (e.g., ball-and-pillow structures), and sand intrusions. The data suggest that during the development of hybrid beds, the lake bottom was commonly covered by a water-rich, unconsolidated (and potentially fluid) mud layer. As mentioned above, McAnally et al. (2007) reported that nonmobile fluid mud is a common feature of eutrophic lake bottoms, where a high content of organic matter hinders consolidation. Such a scenario is probable for the studied Paleogene lake system considering the screening data (average TOC = 2.88 wt%, average HI = 566 mg HC/g TOC, $n = \sim 300$, Petersen et al. 2014), which revealed an elevated content of disseminated amorphous organic matter in the background lake-bottom mud.

The results thus indicate that most of the mud in the density-flow beds was incorporated by erosion into initially turbulent flow in the lake basin.

This strongly supports the previous conceptual models suggesting that muddy sea and lake floor erosion can be a significant process in formation of hybrid beds (e.g., Haughton et al. 2009). This can particularly be the case in systems showing sedimentological evidence of substrate-flow interaction and where hybrid beds contain a transitional-flow division and a thin low-strength-debrite interval that may point to late-stage flow concentration.

Development of the Transitional-Flow Facies

Previous studies have shown that facies transitional between turbidites and debrites are not well understood and most of them are yet to be produced experimentally. Haughton et al. (2009) suggested that the H1–H5 bed divisions record the longitudinal flow evolution of the passing density-flow event, and that the change from H1 to H2 reflects gradual longitudinal change towards the trailing H3. Baas et al. (2011) suggested that H1 and H2 units could be explained by plug-flow dynamics. However, the experimental work of Sumner et al. (2009) studying rapidly decelerating sand- and clay-rich flows and their deposits did not produce any cyclic transitional facies. Similarly, Talling (2013), based on a comprehensive review of ancient occurrences of hybrid beds, concluded that the cyclic H2 unit is lacking or poorly developed in most successions of hybrid beds, and suggested that it is not the norm.

In the Enreca-3 core, the transitional-flow deposits are varied, including sediments showing transitional current ripples and variously developed cyclic banding and lamination (Figs. 9, 14). The transitional-flow facies have a fixed position in the bed motif, occurring above the basal turbulent-flow unit or form the base of the bed. The facies are overlain by inferred upper transitional plug flow (fluid mud) or quasi laminar plug flow (low-strength cohesive debris flow) units. This fixed position suggests that flow dynamics related to the plug-flow development governed their development (Baas and Best 2002; Baas et al. 2009; Baas et al. 2011). The common feature of most of the studied LTPF–UTPF transitional facies is cyclicity. Flume-tank studies of Baas and Best (2002) and Baas et al. (2009) documented that the basal shear layer below the plug flow is influenced by Kelvin-Helmholtz instability characterized by sub-second- to several-seconds-scale fluctuations in turbulence that influences the plug-flow zone. The effect and strength of this instability is varied: the most concentrated of the observed transitional-flow facies in this study, the banded H2 unit, develops under plug flow that reaches a state of low-strength cohesive debris flow in the late stage of flow evolution. In this case, fluctuating turbulence is constantly too suppressed to generate bed forms, but the turbulent pulses can cyclically influence the grain-support capacity of the plug flow. The other banded facies, F5A, develops under major occurrences of incipient plug flow. The sediment concentration of the flow is lower than in flows generating the H2 unit, and cyclic pulses in turbulence lead to an alternation of a ripple-generating turbulent phase (TETF?–LTPF) and a phase of suppressed turbulence, when ripple formation ceases. The smallest scale of the cyclic facies is represented by F3, which develops under small-scale UTPF occurrences. As argued above, these flows must have been slow-moving. The inferred fluctuating turbulence is accordingly weak and generates millimeter- to sub-millimeter-scale interlamination of well-sorted and poorly sorted laminae. Development of ripples (or low-angle cross lamination) was possible during the deposition of F3B, suggesting relatively low sediment concentration, but the nearly flat foreset angle and muddy lithology point to suppressed turbulence. A single occurrence of incipient F3A in the H2 unit supports the interpretation that the processes forming the cyclic transitional facies of various scales are related.

Finally, two intermediate-flow facies (F5A and the smaller-scale F3A) can develop inversely to normally graded lamina sets together with the bounding fluid-mud layers, thus mimicking river-flood-related hyperpycnites (Fig. 8). In this case, however, their origin is linked to changes in

sediment concentration (see also Talling 2014) and shear layer instability developed under the near-bed transitional plug flow (Baas et al. 2009). Screening data (Figs. 8, 15) reveal a significant amount of lacustrine-derived kerogen in a hyperpycnite-like structure, making a direct riverine origin very unlikely.

Depositional System: Apron Sedimentation in a Narrow Syn-Rift Lake?

Due to Neogene inversion, the basin dimensions and source areas are not precisely known. Nevertheless, the seismic data are suggestive of a narrow basin outline (more than ~ 10 km wide) with Paleogene grabens confined by active faults on both sides of the lake (Fig. 2B). Several lines of evidence tentatively suggest that the event sedimentation described here was generated by successive collapses triggered by tectonic instability in the syn-rift lake:

- 1) Occurrence of immature sandstone facies containing angular rock fragments of various origins (Phuong 2014; this study) points to a nearby immature sediment source. Potential candidates for the sediment source include the adjacent rift shoulders.
- 2) The source-rock data summarized above show that most of the organic matter in the event-bed-related mudstones is lacustrine organic matter and not derived from the land.
- 3) The background lacustrine facies indicates that event frequency was typically low: some of the centimeter-scale density-flow beds are directly bounded by varve facies in the upper part of the core. Although systematic varve counting is not possible, the varve facies show that event sedimentation was separated by at least several years of background lacustrine sedimentation. Moreover, even major event beds can be directly overlain by highly oil-prone mudstone with an elevated content of sapropelic organic matter, which is characteristic of this lake system. Considering these data and the limited varve-couplet thickness (commonly 100–500 μm), the lake basin received very limited clastic sediment and input of terrestrial organic matter in between the event-bed sedimentation.
- 4) Hybrid beds (particularly H4–5 units) are often slump folded. This suggests that the hybrid beds are possibly associated with a gradient change.

These data, suggesting short sediment transport distances and an immature sand source, lacustrine mud in event beds, local random interbedding of density-flow deposits and background mudstone, low event frequency, and very limited clastic sedimentation between event deposition, also tentatively suggest that the density flows were mainly associated with aprons and/or ephemeral small deltas, whereas basin-floor fans attached to larger river systems have not been identified from the studied lake system. This interpretation requires testing in future, which should include more systematic screening data from density-flow-bearing para-sequences as well as varve-based estimations of frequency of density-flow events. Apron sedimentation has been reported from a number of rift-lake systems, including modern East Africa, Lake Baikal, and the Paleogene North China Sea (e.g., Nelson et al. 1991; Nelson et al. 1999). The distinction between apron and fan would be relevant considering the major differences in architecture between point-sourced basin-floor fans and linear-sourced aprons (Richards et al. 1998).

Finally, the narrow basin morphology with confining faults on both sides of the lake probably facilitated fast flow deceleration. Together with the assimilation of lake-bottom mud into the density flows, the basin morphology probably played an important role for flow transformation and concentration common for the Enreca-3 deposits (see e.g., Muzzi Magalhaes and Tinterri 2010; Patacci et al. 2014). Moreover, the morphology together with the putative linear-sourced apron sedimentation could explain the locally occurring complex bed motifs (e.g., H2–H3–H2),

which can result from flow reflection and/or simultaneous collapse at various sites along the active faults.

CONCLUSIONS

The Paleogene freshwater rift-lake system reported here records a variety of density-flow types that range from centimeter-scale, mudstone-rich density-flow deposits to meter-scale hybrid beds and debrites. To our knowledge, hybrid beds have not been previously described from freshwater lake systems, yet they can be expected to be a common feature in eutrophic deep rift lakes due to common collapse-related sediment density flows, the soft muddy lake floor, which easily interacts with density flows, and the narrow basin morphology, which favors rapid flow deceleration and concentration. The observation that hybrid beds can be common elements in rift lakes is potentially relevant for understanding reservoir heterogeneities in rift-lake hydrocarbon plays.

The hybrid-bed motifs of the Enreca-3 core include bed motifs essentially similar to those described from marine basins. This suggests that water chemistry has at most only a subordinate influence (and can be masked by factors such as clay mineralogy and content of amorphous organic matter) on flow transformation and concentration, and that hybrid beds of various scales are universal in subaqueous basins.

In addition to hybrid beds, the Enreca-3 deposits are characterized by a wide range of transitional-flow facies at various scales. Facies expressions include transitional current ripples and variously developed cyclic banding and lamination. The beds bearing thinner transitional-flow facies show similarities with beds generated in flume tanks (e.g., Baas et al. 2011), whereas the thicker examples are comparable to beds commonly reported from the rock record. This link is useful, and helps us to extrapolate from experimental data to flows that are of too large scale to be generated in flume tanks. For instance, the transitional-flow facies occupies a fixed position below and/or at plug-flow units in the bed motifs presented here, suggesting that flow dynamics related to plug-flow development governed their development, regardless of the scale of the flow.

Source-rock screening data and sedimentological observations indicate that the lake floor consisted typically of water-rich mud, which was assimilated into overriding density flows. This process was probably central in modulating flow turbulence and explains the pervasive occurrence of transitional-flow facies and indications of late-stage flow concentration. It is possible that such conditions are more common in deep lacustrine basins than in marine basins, but could be probably replicated in certain settings such as ponded fluid-mud-prone basins in the marine realm.

ACKNOWLEDGMENTS

This study forms part of a long-term research cooperation between GEUS, Vietnam Petroleum Institute (VPI), and Danish and Vietnamese universities funded by the Danida, sponsored ENRECA program. PetroVietnam is thanked for significant cosponsoring of the ENRECA-3 well, and the Vietnam Petroleum Institute for logistic and analytical support. Dr. Phach (Hanoi Institute of Oceanography) is thanked for valuable discussions regarding the position of the well. Vietnam Petroleum Institute, PetroVietnam, and GEUS are thanked for permission to publish the results. Dr. Jon Ineson is thanked for his valuable comments on the manuscript. We are very grateful for the constructive reviews by Dr. Zoltan Sylvester, Dr. Brian Romans, and associate editor Dr. Andrea Fildani, which considerably improved the paper. Technical editor Dr. John Southard is thanked for his detailed editing of the final manuscript.

REFERENCES

AMY, L., AND TALLING, P.J., 2006, Anatomy of turbidite and debrite sandstones based on long distance (120 × 35 km) bed correlation, Mamoso Arenacea Formation, Northern Apennines, Italy: *Sedimentology*, v. 53, p. 161–212.

- ANDERSEN, C., MATHIESEN, A., NIELSEN, L.H., TIEM, P.V., PETERSEN, H.I., AND DIEN, P.T., 2005, Distribution of source rocks and maturity modelling in the northern Cenozoic Song Hong Basin (Gulf of Tonkin), Vietnam: *Journal of Petroleum Geology*, v. 28, p. 167–184.
- BAAS, J.H., AND BEST, J.L., 2002, Turbulence modulation in clay-rich sediment-laden flows and some implications for sediment deposition: *Journal of Sedimentary Research*, v. 72, p. 336–340.
- BAAS, J.H., BEST, J.L., PEAKALL, J., AND WANG, M., 2009, A phase diagram for turbulent, transitional and laminar clay suspension flows: *Journal of Sedimentary Research*, v. 79, p. 162–183.
- BAAS, J.H., BEST, J.L., AND PEAKALL, J., 2011, Depositional processes, bedform development and hybrid bed formation in rapidly decelerated cohesive (mud–sand) sediment flows: *Sedimentology*, v. 58, p. 1953–1987.
- BAAS, J.H., MANICA, R., PUHL, E., VERHAGEN, I., AND LUIZA DE O. BORGES, A., 2014, Processes and products of turbidity currents entering soft muddy substrates: *Geology*, v. 42, p. 371–374.
- BARKER, S.P., HAUGHTON, P.D.W., MCCAFFREY, W.D., ARCHER, S.G., AND HAKES, B., 2008, Development of rheological heterogeneity in clay-rich high-density turbidity currents: Aptian Britannia Sandstone Member, UK Continental Shelf: *Journal of Sedimentary Research*, v. 78, p. 45–68.
- BOHACS, K.M., CARROLL, A.R., NEAL, J.E., AND MANKIEWICZ, P.J., 2000, Lake basin type, source potential, and hydrocarbon character: an integrated sequence-stratigraphic–geochemical framework: *American Association of Petroleum Geologists, Studies in Geology* 46, p. 3–34.
- BORDENAVE, M.L., ESPITALIÉ, J., LEPLAT, P., OUDIN, J.L., AND VANDENBROUCK, M.L., 1993, Screening techniques for source rock evaluation, *in* Bordenave, M., ed., *Applied Petroleum Geochemistry: Editions Technip*, p. 219–278.
- BOUMA, A.H., 1962, *Sedimentology of Some Flysch Deposits: A Graphic Approach to Facies Interpretation*: Amsterdam, Elsevier, 168 p.
- BUTLER, R.W.H., EGGENHUISEN, J.T., HAUGHTON, P., AND MCCAFFREY, W.D., 2016, Interpreting syndepositional sediment remobilization and deformation beneath submarine gravity flows: a kinematic boundary layer approach: *Geological Society of London, Journal*, v. 173, p. 46–58.
- CARROLL, A.R., AND BOHACS, K.M., 2001, Lake type control on petroleum source rock potential in nonmarine basins: *American Association of Petroleum Geologists, Bulletin*, v. 85, p. 1033–1053.
- FYHN, M.B.W., *in review*, Linking Paleogene rifting and inversion in the northern Song Hong and Beibuwan basins, Vietnam, with left-lateral motion on the Ailao Shan–Red River Shear Zone: submitted to, Çemen, I., and Summa, L.L., eds., *Rift Systems: American Association of Petroleum Geologists, Memoir* 115.
- FYHN, M.B.W., AND PHACH, P.V., 2015, Late Neogene structural inversion around the northern Gulf of Tonkin, Vietnam: effects from right-lateral displacement across the Red River fault zone: *Tectonics*, v. 34, p. 290–312.
- HAUGHTON, P.D.W., BARKER, S.P., AND MCCAFFREY, W., 2003, “Linked” debrites in sand-rich turbidite systems: origin and significance: *Sedimentology*, v. 50, p. 459–482.
- HAUGHTON, P.D.W., DAVIS, C., MCCAFFREY, W., AND BARKER, S.P., 2009, Hybrid sediment gravity flow deposits: classification, origin and significance: *Marine and Petroleum Geology*, v. 26, p. 1900–1918.
- HODGSON, D.M., 2009, Distribution and origin of hybrid beds in sand-rich submarine fans of the Tanqua depocentre, Karoo Basin, South Africa: *Marine and Petroleum Geology*, v. 26, p. 1940–1956.
- HUANG, B., TIAN, H., WILKINS, R.W.T., XIAO, X., AND LI, L., 2013, Geochemical characteristics, palaeoenvironment and formation model of Eocene organic-rich shales in the Beibuwan Basin, South China Sea: *Marine and Petroleum Geology*, v. 48, p. 77–89.
- ICHASO, A.A., AND DALRYMPLE, R.W., 2009, Tide- and wave-generated fluid mud deposits in the Tilje Formation (Jurassic), offshore Norway: *Geology*, v. 37, p. 539–542.
- ILSTAD, T., ELVERHØI, A., ISSLER, D., AND MARR, J.G., 2004, Subaqueous debris flow behaviour and its dependence on the sand/clay ratio: a laboratory study using particle tracking: *Marine Geology*, v. 213, p. 415–438.
- ITO, M., 2008, Downfan transformation from turbidity currents to debris flows at a channel-lobe transitional zone: the Lower Pleistocene Otadai Formation, Boso Peninsula, Japan: *Journal of Sedimentary Research*, v. 78, p. 668–682.
- KANE, I.A., AND PONTEN, A.S.M., 2012, Submarine transitional flow deposits in the Paleogene Gulf of Mexico: *Geology*, v. 40, p. 1119–1122.
- LOWE, D.R., 1982, Sediment gravity flows, II. Depositional models with special reference to high density turbidity currents: *Journal of Sedimentary Petrology*, v. 52, p. 279–298.
- LOWE, D.R., AND GUY, M., 2000, Slurry-flow deposits in the Britannia Formation (Lower Cretaceous), North Sea: a new perspective on the turbidity current and debris flow problem: *Sedimentology*, v. 47, p. 31–70.
- LOWE, D.R., GUY, M., AND PALFREY, A., 2003, Facies of slurry-flow deposits, Britannia Formation (Lower Cretaceous), North Sea: implications for flow evolution and deposit geometry: *Sedimentology*, v. 50, p. 45–80.
- MCCAVE, I.N., AND JONES, K.P.N., 1988, Deposition of ungraded muds from high-density non-turbulent turbidity currents: *Nature*, v. 333, p. 250–252.
- MACKAY, D.A., AND DALRYMPLE, R.W., 2011, Dynamic mud deposition in a tidal environment: the record of fluid-mud deposition in the Cretaceous Bluesky Formation, Alberta, Canada: *Journal of Sedimentary Research*, v. 81, p. 901–920.
- MACQUAKER, J.H.S., BENTLEY, S.J., AND BOHACS, K.M., 2010, Wave-enhanced sediment-gravity flows and mud dispersal across continental shelves: reappraising sediment

- transport processes operating in ancient mudstone successions: *Geology*, v. 38, p. 947–950.
- MCANALLY, W.H., FRIEDRICH, C., HAMILTON, D., HAYTER, E., SHRESTHA, P., RODRIGUEZ, H., SHERMET, A., AND TEETER, A., 2007, Management of fluid mud in estuaries, bays, and lakes. I: Present state of understanding on character and behaviour: *Journal of Hydraulic Engineering*, v. 133, p. 9–22.
- MUZZI MAGALHAES, P., AND TINTERRI, R., 2010, Stratigraphy and depositional setting of slurry and contained (reflected) beds in the Marnoso-arenacea Formation (Langhian–Serravallian) Northern Apennines, Italy: *Sedimentology*, v. 57, p. 1685–1720.
- NELSON, C.H., MALDONADO, A., BARBER, J.H., AND ALONSO, B., 1991, Modern sand-rich and mud-rich siliciclastic aprons, alternative base-of-slope turbidite systems to submarine fans, in Weimer, P., and Link, M.H., eds., *Seismic Facies and Sedimentary Processes of Submarine Fans and Turbidite Systems*: New York, Springer-Verlag, *Frontiers in Sedimentary Geology*, p. 171–190.
- NELSON, C.H., KARABANOVA, E.B., COLMAN, S.M., AND ESCUTIA, C., 1999, Tectonic and sediment supply control of deep rift lake turbidite systems: Lake Baikal, Russia: *Geology*, v. 27, p. 163–166.
- NIELSEN, L.H., MATHIESEN, A., BIDSTRUP, T., VEJBEK, O.V., DIEN, P.T., AND TIEM, P.V., 1999, Modelling of hydrocarbon generation in the Cenozoic Song Hong Basin, Vietnam: a highly prospective basin: *Journal of Asian Earth Sciences*, v. 17, p. 269–294.
- PATACCI, M., HAUGHTON, P., AND MCCAFFREY, W.D., 2014, Rheological complexity in sediment gravity flows forced to decelerate against a confining slope, Braux, SE France: *Journal of Sedimentary Research*, v. 84, p. 270–277.
- PETERS, K.E., AND CASSA, M.R., 1994, Applied source rock geochemistry, in Magoon, L.B., and Dow, W.G., eds., *The Petroleum System: from Source to Trap*: American Association of Petroleum Geologists, *Memoir 60*, p. 93–120.
- PETERSEN, H.I., TRU, V., NIELSEN, L.H., DUC, N.A., AND NYTOFT, H.P., 2005, Source rock properties of lacustrine mudstones and coals (Oligocene Dong Ho Formation), onshore Song Hong Basin, northeastern Vietnam: *Journal of Petroleum Geology*, v. 28, p. 19–38.
- PETERSEN, H.I., FYHN, M.B.W., NIELSEN, L.H., TUAN, H.A., QUANG, C.D., TUYEN, N.T., THANG, P.V., THAM, N.T., OANG, N.K., AND ABATZIS, I., 2014, World-class Paleogene oil-prone source rocks from a cored lacustrine syn-rift succession, Bach Long Vi Island, Song Hong Basin, offshore Northern Vietnam: *Journal of Petroleum Geology*, v. 37, p. 373–389.
- PHUONG, B.T.N., 2014, Petrographic characteristics and reservoir quality of sandstone reservoirs from Enreca-3 well in Bach Long Vi island: *PetroVietnam Journal*, v. 10, p. 39–44.
- PIASECKI, S., CHRISTIANSEN, F.G., AND STEMMERIK, L., 1990, Depositional history of a Late Carboniferous organic rich shale from East Greenland: *Bulletin of Canadian Petroleum Geology*, v. 38, p. 273–287.
- POWER, B., COVAULT, J., FILDANI, A., SULLIVAN, M., CLARK, J., CARSON, B., ZARRA, L., AND ROMANS, B., 2013, Facies analysis and interpretation of argillaceous sandstone beds in the Paleogene Wilcox Formation, deepwater Gulf of Mexico: *Gulf Coast Association of Geological Societies, Transactions*, v. 63, p. 575–578.
- RICHARDS, M., BOWMAN, B., AND READING, H., 1998, Submarine fan systems I: characterization and stratigraphic prediction: *Marine and Petroleum Geology*, v. 15, p. 578–606.
- SCHIEBER, J., SOUTHARD, J.B., AND THAISEN, K., 2007, Accretion of mudstone beds from migrating floccule ripples: *Science*, v. 318, p. 1760–1763.
- STEVENSON, C.J., TALLING, P.J., MASSON, D.G., SUMNER, E.J., FRENZ, M., AND WYNN, R.B., 2014, The spatial and temporal distribution of grain-size breaks in turbidites: *Sedimentology*, v. 61, p. 1120–1156.
- SUMNER, E.J., TALLING, P.J., AND AMY, L.A., 2009, The deposits of flows transitional between turbidity currents and debris flow: *Geology*, v. 37, p. 991–994.
- SUMNER, E.J., TALLING, P.J., AMY, L.A., WYNN, R.B., STEVENSON, C., AND FRENZ, M., 2012, Facies architecture of individual basin-plain turbidites: comparison with existing models and implications for flow processes: *Sedimentology*, v. 59, p. 1850–1857.
- SYLVESTER, Z., AND LOWE, D.R., 2004, Textural trends in turbidites and slurry beds from the Oligocene flysch of the Carpathians, Romania: *Sedimentology*, v. 51, p. 945–972.
- TALLING, P.J., 2013, Hybrid submarine flows comprising turbidity current and cohesive debris flow: deposits, theoretical and experimental analyses, and generalized models: *Geosphere*, v. 9, p. 1–28.
- TALLING, P.J., 2014, On the triggers, resulting flow types and frequencies of subaqueous sediment density flows in different settings: *Marine Geology*, v. 352, p. 155–182.
- TALLING, P.J., AMY, L.A., WYNN, R.B., PEAKALL, J., AND ROBINSON, M., 2004, Beds comprising debrite sandwiched within co-genetic turbidite: origin and widespread occurrence in distal depositional environments: *Sedimentology*, v. 51, p. 163–194.
- TALLING, P.J., MALGESINI, G., SUMNER, E.J., AMY, L.A., FELLETTI, F., BLACKBOURN, G., NUTT, C., WILCOX, C., HARDING, I.C., AND KHAN, S., 2012a, Planform geometry, stacking pattern, and extra-basinal origin of low-strength and intermediate-strength cohesive debris flow deposits in the Marnoso-arenacea Formation: *Geosphere* v. 8, p. 1–24.
- TALLING, P.J., SUMNER, E.J., MASSON, D.G., AND MALGESINI, G., 2012b, Subaqueous sediment density flows: Depositional processes and deposit types: *Sedimentology*, v. 59, p. 1937–2003.
- TERLAKY, V., AND ARNOTT, W., 2014, Matrix-rich and associated matrix-poor sandstones: avulsion splays in slope and basin-floor strata: *Sedimentology*, v. 61, p. 1175–1197.
- TRAER, M., HILLEY, G.E., FILDANI, A., AND MCHARGUE, T.R., 2012, The sensitivity of turbidity currents to mass and momentum exchanges between these underflows and their surroundings: *Journal of Geophysical Research*, v. 117, F01009, p. 1–16.
- TRAER, M., FILDANI, A., AND MCHARGUE, T.R., AND HILLEY, G.E., 2015, Simulating depth-averaged, one-dimensional turbidity current dynamics using natural topographies: *Journal of Geophysical Research*, v. 120, p. 1485–1500.
- VERHAGEN, I.T.E., BAAS, J.H., JACINTO, R.S., MCCAFFREY, W.D., AND DAVIES, A.G., 2013, A first classification scheme of flow-bed interaction for clay-laden density currents and soft substrates: *Ocean Dynamics*, v. 63, p. 385–397.

Received 2 July 2015; accepted 18 April 2016.